Formation and temperature dependence of Highly Oxygenated Organic Molecules (HOM) from Δ^3-carene ozonolysis

Yuanyuan Luo[1*], Ditte Thomsen[2], Emil Mark Iversen[2], Pontus Roldin[3,4], Jane Tygesen Skønager[2], Linjie Li[5], Michael Priestley[5], Henrik B. Pedersen[6], Mattias Hallquist[5], Merete Bilde[2], Marianne Glasius[2], and Mikael Ehn[1*]

[1]Institute for Atmospheric and Earth System Research (INAR), University of Helsinki, Helsinki, 000149, Finland
[2]Department of Chemistry, Aarhus University, Aarhus C, 8000, Denmark
[3]Department of Physics, Lund University, Lund, 22100, Sweden
[4]IVL, Swedish Environmental Research Institute, SE-211 19 Malmö, Sweden
[5]Department of Chemistry and Molecular Biology, University of Gothenburg, Gothenburg, 41296, Sweden
[6]Department of Physics and Astronomy, Aarhus University, Aarhus C, 8000, Denmark

Correspondence to: Yuanyuan Luo (yuanyuan.luo@helsinki.fi) and Mikael Ehn (mikael.ehn@helsinki.fi)

Keywords: HOM, Δ^3-carene oxidation, temperature dependence, RH effect, ADCHAM model

Abstract.

Δ^3-carene is a prominent monoterpene in the atmosphere, contributing significantly to secondary organic aerosol (SOA) formation. However, knowledge about Δ^3-carene oxidation pathways, particularly regarding its ability to form highly oxygenated organic molecules (HOM), is still limited. In this study, we present HOM measurements during Δ^3-carene ozonolysis under various conditions in two simulation chambers. We identified numerous HOM (monomers: $C_{7-10}H_{10-18}O_{6-14}$, dimers: $C_{17-20}H_{24-34}O_{6-18}$) using a chemical ionization mass spectrometer (CIMS). Δ^3-carene ozonolysis yielded higher HOM concentrations than α-pinene, with a distinct distribution, indicating differences in formation pathways. All HOM signals decreased considerably at lower temperatures, reducing the estimated molar HOM yield from ~3 % at 20 °C to ~0.5 % at 0 °C. Interestingly, temperature change altered the HOM distribution, increasing the observed dimer-to-monomer ratios from roughly 0.8 at 20 °C to 1.5 at 0 °C. HOM monomers with 6 or 7 O-atoms condensed more efficiently onto particles at colder temperatures, while monomers with nine or more O-atoms and all dimers condensed irreversibly even at 20 °C. Using the gas- and particle-phase chemistry kinetic multilayer model ADCHAM, we were also able to reproduce the experimentally observed HOM composition, yields and temperature dependence.

1. Introduction

Secondary organic aerosol (SOA), formed through gas-to-particle conversion in the atmosphere, constitutes a major contributor to the global submicron aerosol mass (Hallquist et al., 2009). Atmospheric SOA formation has important implications for the climate and human health (Shiraiwa et al., 2017; Cohen et al., 2017; Shrivastava et al., 2017; Jimenez et al., 2009). The largest precursor of SOA is biogenic volatile organic compounds (BVOCs), which are emitted naturally by vegetation and dominate global VOC emissions (Guenther et al., 2012). In the ambient air, BVOCs can react with a variety of oxidants, such as ozone (O_3), hydroxyl radical (OH), or nitrate radical (NO_3), to produce more functionalized organic products. Highly oxygenated organic molecules (HOM) are a recently identified group of VOC oxidation products formed through rapid autoxidation processes in the atmosphere (Ehn et al., 2014; Bianchi et al., 2019). Containing six or more oxygen atoms, HOM are typically highly oxidized and functionalized species with low volatilities, making them crucial in SOA formation through condensation or reactive uptake (Ehn et al., 2014; Bianchi et al., 2019; Bianchi et al., 2016).

Monoterpenes ($C_{10}H_{16}$) account for approximately 15% of the annual global BVOCs emissions (Guenther et al., 2012). Previous studies have reported a broad range of SOA yields resulting from monoterpene oxidation, with values spanning from less than 1% to over 60% (Saathoff et al., 2009; Warren et al., 2009; Ehn et al., 2014; Hallquist et al., 1999; Kristensen et al., 2020; Thomsen et al., 2022). This variation highlights the significant disparities in monoterpene oxidation mechanisms and the potential of their products to form SOA under different conditions. The most abundantly emitted monoterpene, α-pinene, has been the subject of numerous laboratory and field studies (e.g. Ehn et al. (2014); Berndt et al. (2003); Zhao et al. (2023); Molteni et al. (2019); Tillmann et al. (2010); Kristensen et al. (2020)). Many modellers have also employed α-pinene as a representative compound for endocyclic monoterpenes in the regional or global aerosol budget (Boy et al., 2013; Pye et al., 2010). To date, however, the fate of other monoterpenes in the atmosphere remains less understood, and evaluating the variability of their impact on SOA formation continues to be a challenge.

Δ^3-carene is a bicyclic unsaturated monoterpene (Scheme 1), distinguished from α-pinene's structure primarily by its 3-membered ring. Despite being predicted to have lower emissions than α-pinene at a global scale (Sindelarova et al., 2014), Δ^3-carene has been measured in equivalent proportions in ambient air in certain regions (Fry et al., 2013; Kim et al., 2013; Geron et al., 2000; Bäck et al., 2012). SOA yields from photochemical oxidation of Δ^3-carene have been determined to be 2 - 38% (Hoffmann et al., 1997; Griffin et al., 1999; Lee et al., 2006), and D'Ambro et al. (2022) detected both gas- and particle-phase products from OH oxidation of Δ^3-carene and developed a mechanism for the initial stage of carene-OH oxidation with the support of computational chemistry. Recently, experimental and theoretical research on HOM formation from NO_3 oxidation of Δ^3-carene has also been carried out (Dam et al., 2022; Draper et al., 2019; Liu et al., 2022; Day et al., 2022), and it has been suggested that the higher SOA yield from NO_3-initiated oxidation of Δ^3-carene (15%-65%) compared with α-pinene (0-16%) (Hallquist et al., 1999; Fry et al., 2014) might be due to differences in the potential for further radical propagation and oxidation of the first-generation radicals from early unimolecular processes. The ozonolysis of Δ^3-carene is also of particular importance as this process can contribute to both SOA and OH formation in the atmosphere. Previous studies have reported that Δ^3-carene

ozonolysis has similar or slightly higher SOA yields compared to α-pinene ozonolysis under similar conditions (Thomsen et al., 2021; Thomsen et al., 2022). Several studies have measured various less-oxidized products (e.g. organic acids) from Δ^3-carene ozonolysis and explored their possible formation pathways (Wang et al., 2019; Glasius et al., 2000; Baptista et al., 2014; Ma et al., 2009). However, very little is currently known about the HOM formation resulting from O_3-initiated Δ^3-carene oxidation (Li et al., 2019; Mentel et al., 2015), the only source providing HOM spectra from Δ^3-carene ozonolysis is the study by Li et al. (2019).

In this study, we conducted a series of chamber experiments to investigate the HOM formation from Δ^3-carene ozonolysis with and without the presence of an OH scavenger. We present the differences in HOM formation between Δ^3-carene and α-pinene ozonolysis concerning potential pathways, molar yield, and composition. Additionally, we estimate the relative volatilities of the detected HOM species to qualitatively assess their contributions to SOA formation. We also explored the impact of temperature on the composition and distribution of HOM. Finally, the aerosol dynamics and gas- and particle-phase chemistry kinetic multilayer model ADCHAM (Roldin et al., 2019; Roldin et al., 2014) was utilized to simulate the HOM formation from Δ^3-carene ozonolysis to compare to our experimental results.

2. Materials and Methods

2.1. Chamber facilities and instrumentation

Δ^3-carene ozonolysis experiments were performed in two different chambers: (a) the COALA chamber at University of Helsinki, Finland, to assess HOM compositions and their potential formation pathways, and (b) the AURA chamber at Aarhus University in Denmark, to investigate the impact of temperature and relative humidity (RH) on HOM formation.

The COALA chamber is a 2 m^3 Teflon reactor maintained at room temperature (25 ± 1℃) under dry conditions (RH < 1%). During this campaign, the chamber was run in continuous mode with a total inflow of 40 L min^{-1} (average residence time: ~ 50 min). We conducted eleven Δ^3-carene ozonolysis experiments under different oxidation conditions (Table S1). A proton transfer reaction time-of-flight mass spectrometer (PTR-TOF 8000, Ionicon Analytik Gmbh) was deployed to measure VOC concentrations, while a chemical ionization atmospheric pressure interface time-of-flight mass analyser (CIMS, Tofwerk AG/Aerodyne Research, Inc.) with nitrate (NO_3^-) as the reagent ion (hereafter NO_3-CIMS) was employed to probe oxygenated products from Δ^3-carene ozonolysis, with a primary focus on HOM. In this paper, the signal intensity of species detected with NO_3-CIMS is presented as a normalized signal, which refers to the raw signal intensity normalized to the reagent ions, unless specified otherwise.

The AURA chamber is a 5 m^3 Teflon chamber situated in a temperature-controlled room (temperature range: -16 – 26 ℃). Throughout the campaign, the AURA chamber was run in batch mode, meaning that all reagents are injected in a single batch at the start of the experiment and products accumulate progressively. As shown in Table S2, the HOM formation of Δ^3-carene ozonolysis was examined under dry conditions (RH < 15%) at 20 ℃ (20A & B), 10 ℃ (10A & B), and 0 ℃ (0A), and twice under humid conditions (RH = 80%) at 10 ℃ with two different Δ^3-carene loadings (10D: 10 ppb and 10 E: 20 ppb). The

experiment commenced with the introduction of Δ^3-carene into the chamber, marking the time as experiment time = 0 min. Instruments for both gas phase and particle phase measurements were deployed. For HOM measurement, a same type of NO$_3$-CIMS as employed in the COALA lab was utilized.

95 Note that in this paper we, in accordance with most previous studies, term the set of compounds that we observe with the NO$_3$-CIMS that match the Bianchi et al. (2019) criteria as HOM. These are species containing six or more oxygen atoms, formed in the gas phase via autoxidation involving peroxy radicals (RO$_2$) under atmospherically relevant conditions. It is acknowledged, however, that some compounds may not be detected or are detected with lower sensitivity. The schematic of these two chambers is shown in Figure S1, and more details of the set-ups and instruments are provided in Section S1.

100 Importantly, the differences between batch- and continuous-mode chamber experiments are described there.

2.2. Δ^3-carene ozonolysis chemistry

For the purpose of interpreting our mass spectral observations, we here provide a brief overview of the main reaction pathways from the ozonolysis of Δ^3-carene. An initial addition of O$_3$ to the double bond (Scheme 1) results in Criegee Intermediates (CI) that undergo unimolecular isomerization followed by OH loss and O$_2$ addition, forming "primary" RO$_2$ with an elemental

105 composition of C$_{10}$H$_{15}$O$_4$. With a suitable structure, RO$_2$ intramolecular H-shifts and O$_2$ addition (i.e. autoxidation) can take place, leading to high oxygen content of the formed RO$_2$ (C$_{10}$H$_{15}$O$_{even}$). The reaction between Δ^3-carene and O$_3$ also produces OH, as depicted in Scheme 1, and the OH yields were reported to be 0.56-1.1 by previous studies (Wang et al., 2019; Hantschke et al., 2021; Atkinson et al., 1992; Aschmann et al., 2002). OH can react with Δ^3-carene as well, where it can either attach to the double bond, resulting in an initial RO$_2$ as C$_{10}$H$_{17}$O$_3$, or abstract a hydrogen atom to form an RO$_2$ as C$_{10}$H$_{15}$O$_2$. Subsequent

110 autoxidation is expected to produce RO$_2$ with the formulas of C$_{10}$H$_{17}$O$_{odd}$ and C$_{10}$H$_{15}$O$_{even}$ from addition and abstraction, respectively. However, it should be noted that for VOCs with double bonds, the OH-abstraction pathway is not typically significant (Atkinson and Arey, 2003), and the dominant source of C$_{10}$H$_{15}$O$_{even}$ will be the ozone reactions.

Highly oxidized RO$_2$ can terminate to closed-shell compounds, i.e., HOM monomers or HOM dimers via either unimolecular decomposition (typically R1) or by bimolecular reactions with other RO$_2$ (R2-R5) and hydroperoxyl radicals (HO$_2$ (R6-R8) in

115 our system.

$$RO_2 \rightarrow R'_{-H}=O + OH \qquad\qquad (R1)$$

When RO$_2$ reacts with other RO$_2$, a tetroxide intermediate is formed and rapidly decomposes to a complex of two alkoxy radicals (RO) and releases an oxygen molecule. The RO complex can then undergo different processes resulting in various products. First, the complex can directly decompose to two RO (R2), which subsequently generate closed-shell species after

120 HO$_2$-loss (R9) or alkyl radicals via channels R10,11. The alkyl radicals related to R10,11 pathways can either terminate unimolecularly, or ultimately reform a new RO$_2$. For example, C$_{10}$H$_{15}$O$_{odd}$ and C$_{10}$H$_{17}$O$_{even}$ can be formed from reactions of C$_{10}$H$_{15}$O$_{even}$ and C$_{10}$H$_{17}$O$_{odd}$ via reactions R2 + R10,11. Second, the RO complex can decompose to a carbonyl and an alcohol, as simplified in Reaction R3 (Vereecken and Peeters, 2009). Third, two RO of the complex can recombine into a ROOR' accretion product (i.e., HOM dimer) (Hasan et al., 2020) after intersystem crossing (R4). To illustrate, the reactions between

O3-initiated RO_2 $C_{10}H_{15}O_{even}$ and OH-initiated RO_2 $C_{10}H_{17}O_{odd}$ would produce $C_{20}H_{30,34}O_{even}$ and $C_{20}H_{32}O_{odd}$ dimers, depending on the RO_2 combinations. Finally, the RO complex could also undergo other untypical reactions (R5) for example β scission of one RO in the complex (Peräkylä et al., 2023) which are unique for RO with suitable structures.

$$RO_2 + R'O_2 \rightarrow ROOOOR' \xrightarrow{-O_2} RO{\cdots}OR' \rightarrow RO + R'O \qquad (R2)$$

$$\rightarrow ROH + R'_{-H}C{=}O \qquad (R3)$$

$$\rightarrow RO{\cdots}OR' \qquad (R4)$$

$$\rightarrow \text{other products} \qquad (R5)$$
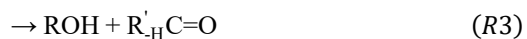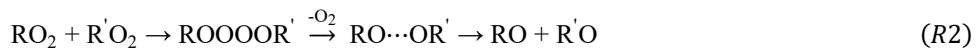
Similar to the reactions of two RO_2, the reactions of RO_2 with HO_2 can lead to either termination (R6,7) (Groß et al., 2014; Praske et al., 2015; Schwantes et al., 2015) or radical propagation (R8) (Hasson et al., 2005). It is generally expected that HO_2 reactions terminate autoxidation following the reaction channel R6. However, other reaction channels also play a significant role for more complex RO_2, e.g. reaction channel R8 was found to have a high yield for acylperoxy radicals (Groß et al., 2014; Hasson et al., 2005). Therefore, for example, it is theoretically possible that O3-initiated RO_2 $C_{10}H_{15}O_{even}$ can form closed-shell monomers $C_{10}H_{16}O_x$ or generate new RO_2 $C_{10}H_{15}O_{odd}$ via different reactions with HO_2. Note that in this study, the reactions of RO_2 with HO_2 were expected to prevail only when CO was injected into the chamber.

$$RO_2 + HO_2 \rightarrow ROOH + O_2 \qquad (R6)$$

$$\rightarrow ROH + O_3 \qquad (R7)$$

$$\rightarrow RO + OH + O_2 \qquad (R8)$$

$$RO + O_2 \rightarrow R'_{-H}{=}O + HO_2 \qquad (R9)$$

$$RO \xrightarrow{\text{scission}} \text{products} \qquad (R10)$$

$$\xrightarrow{\text{H-shift isomerization}} \text{products} \qquad (R11)$$
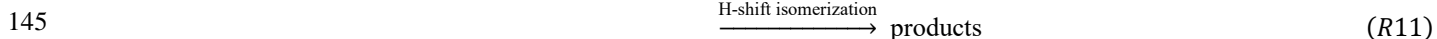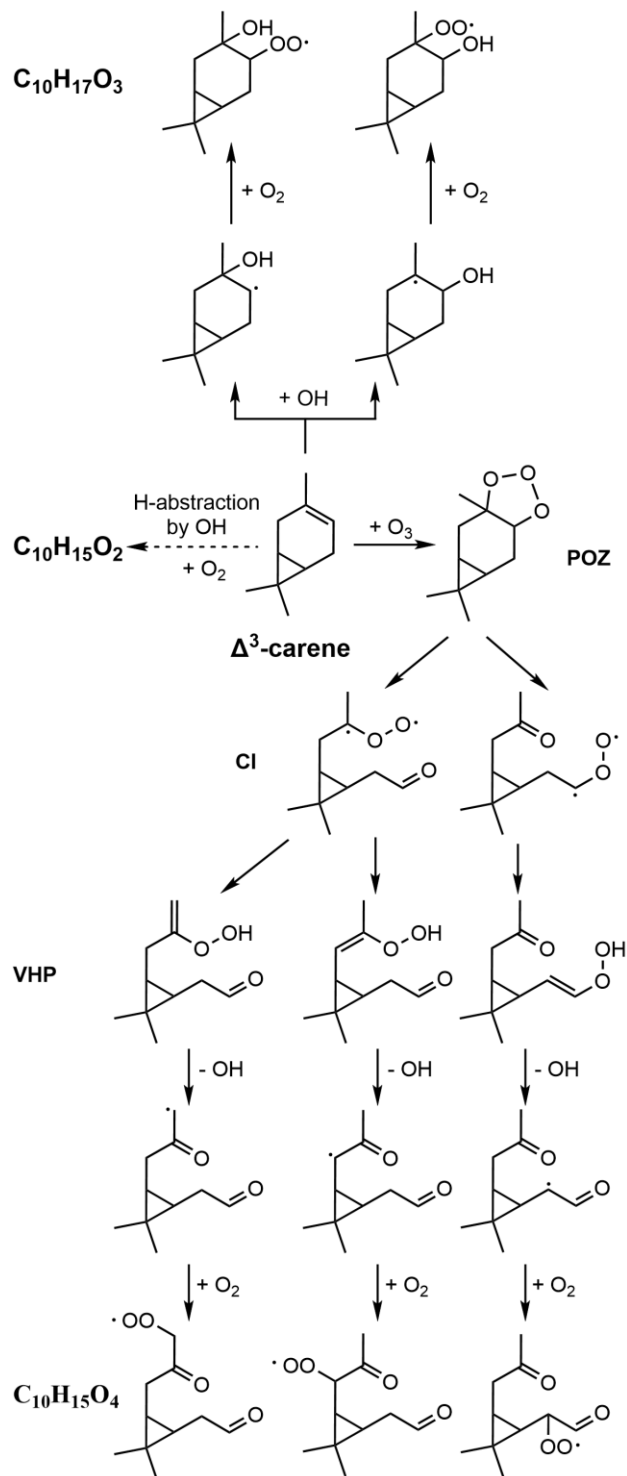
Scheme 1. Simplified formation mechanism of the different primary RO_2 from ozone and OH initiated oxidation of Δ^3-carene. POZ: cyclic primary ozonide; CI: Criegee intermediates; VHP: vinyl hydroperoxides.

2.3. ADCHAM modelling

We used the ADCHAM model to simulate the gas-phase chemistry, HOM formation and SOA formation during the AURA and COALA experiments. The general model setup, aerosol dynamics and predicted SOA formation during the experiments are described by Thomsen et al. (2024). Here we only describe the new Δ^3-carene gas phase oxidation mechanism that was implemented in ADCHAM. ADCHAM incorporates a comprehensive model for autoxidation and HOM formation for α-pinene, serving as the foundational basis for carene ozonolysis model. In this study, we updated the ADCHAM model drawing upon prior research on the ozonolysis and OH-oxidation of Δ^3-carene (D'Ambro et al., 2022; Hantschke et al., 2021; Wang et al., 2019), alongside HOM and SOA data from our campaign. The first generation reaction rates and branching ratios of the implemented Δ^3-carene gas-phase chemistry mechanism is based on the theoretical work on ozonolysis of Δ^3-carene by Wang et al. (2019) and the experimental work on ozonolysis and OH-oxidation of Δ^3-carene by Hantschke et al. (2021). According to the theoretical work by Wang et al. (2019) four different Criegee intermediate (CI) conformers are formed during the ozonolysis of Δ^3-carene. These CIs undergo prompt unimolecular reactions to form secondary ozonides (SOZs), vinyl hydroperoxides (VHPs), dioxiranes (DIOs) and stabilized CIs (SCIs). The VHPs decomposes rapidly and form RO_2 and OH while the SOZs can isomerize promptly to 3-caronic acid. According to the calculations by Wang et al. (2019) the VHP and OH yield during the ozonolysis of Δ^3-carene is ~56 %, the SOZs yield (3-caronic acid yield) is ~24 %, the DIOs yield is 16 % and the SCIs yield is 4 %. The theoretically derived OH yield from Wang et al. (2019) is in reasonable agreement with the experimentally derived OH yield of 65 % by Hantschke et al. (2021). Since the existence and fate of dioxiranes are largely unknown (Hantschke et al., 2021) we exclude the proposed reaction pathways leading to these products in the present work. Instead, we assume that the initial CIs exclusively decomposes to 65 % VHPs and 35 % SOZs, which result in final first-generation ozonolysis product yields of 65 % RO_2 + OH and 35 % 3-caronic acid.

The first-generation RO_2 is distributed among four distinct isomers. It is hypothesized that one major RO_2 isomer, analogous to the first-generation α-pinene ozonolysis product C109O2 in MCMv3.3.1 and named D3C109O2, predominates with a molar yield (branching ratio) of 96.2%. The remaining three isomers represent $C10$ RO_2 that can undergo autoxidation of peroxy radicals, thereby forming HOM, as detailed in Table S6. In addition, we have included a minor route to C_9 RO_2 that can undergo peroxy radical autoxidation. These C_9 RO_2 are expected to be formed as a second-generation bimolecular reaction product when D3C109O2 reacts with other RO_2 or NO. To capture the observed profound impact of CO on the HOM mass spectrum evolution in COALA, the lower RO_2+RO_2 reaction rates (on the order of ~5 times lower) for Δ^3-carene than in earlier peroxy radical autoxidation mechanism (PRAM) (Roldin et al., 2019; Nie et al., 2023) were utilized. Otherwise, the RO_2+RO_2 termination reactions are still dominating over the RO_2+HO_2 reactions after the CO addition in COALA, when assigning the MCM generic rate coefficient $KRO2HO2 \approx 2 \times 10^{-11}$ molec^{-1} cm^3 s^{-1} for all RO_2+HO_2 reactions in the model. Additionally, we accounted for different RO_2+HO_2 reaction pathways (R6-R8) in this presented Δ^3-carene mechanism while in previous monoterpene PRAM (Roldin et al., 2019; Nie et al., 2023), all RO_2+HO_2 reactions resulted in closed shell HOM ROOH ($C_{10}H_{16}O_x$) (R6). The molar yield of the 4 RO_2 that can undergo autoxidation are summarized in Table S3. Table S4 provide

the Δ^3-carene ozone chemistry mechanism, excluding the PRAM and Table S5 the Δ^3-carene OH-oxidation mechanism. Table S6 and Table S7 list all PRAM reactions. The full mechanism, in a format compatible with the kinetic pre-processor, will be provided upon publication in an open access repository at Zenodo.

3. Results and Discussion

3.1. HOM formation and general features
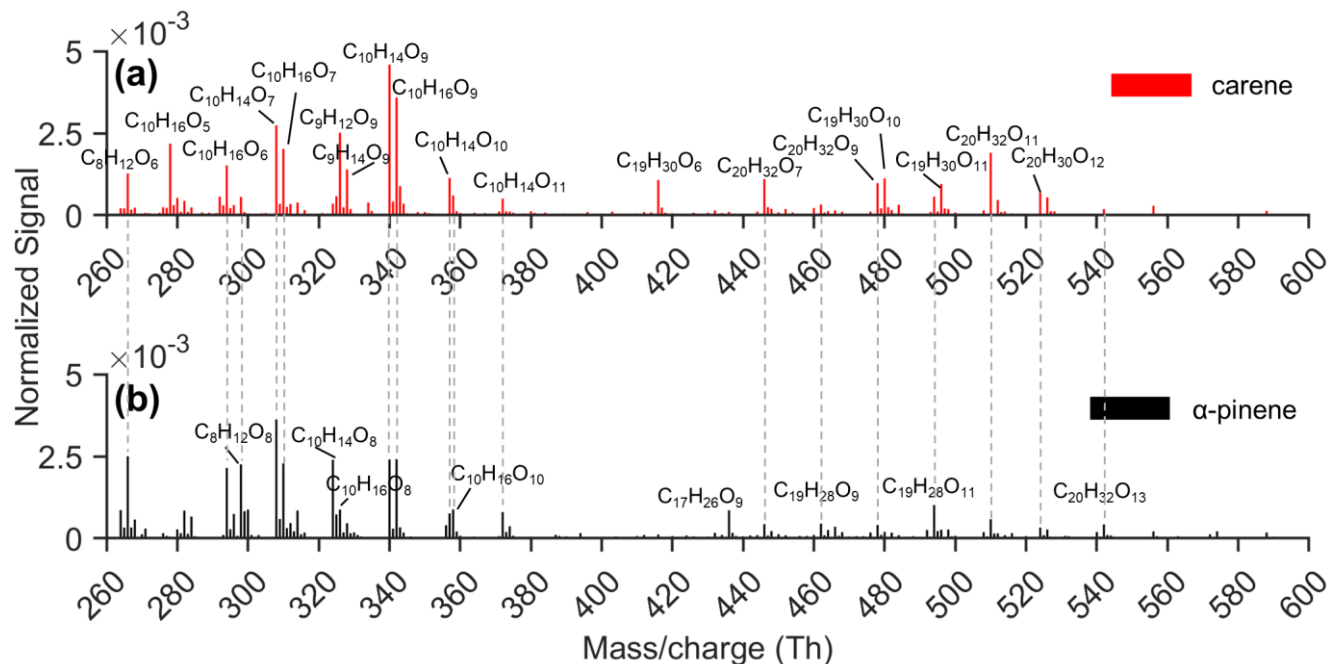
Figure 1. UMR (unit-mass resolution) mass spectra from (a) Δ^3-carene (a) and (b) α-pinene ozonolysis in the COALA chamber under the same conditions (VOC = 20 ppb, O_3 = 30 ppb). All peaks labelled were detected as a cluster with NO_3^-, and the gray dashed lines mark some of the products with the same formulas detected both in Δ^3-carene and α-pinene ozonolysis experiments.

During our experiments in the COALA chamber, numerous HOM with a broad oxygenation pattern were observed as nitrate adducts in the mass range from 260 Th to 600 Th as illustrated in Figure 1(a). The spectra observed in our study are similar to those reported by Li et al. (2019) , who conducted $\Delta3$-carene ozonolysis under high concentrations (VOC: ~1100 ppb; O_3: ~900 ppb) at room temperature and dry conditions. Both studies identified predominant monomers as $C_{10}H_{14,16}O_{7,9}$ in both spectra, and the most abundant dimer groups as $C_{20}H_{32}O_{7,9,11}$ and $C_{19}H_{30}O_{6,10,11}$. However, the relative abundances of the dominant species differed slightly. For instance, $C_{20}H_{32}O_{11}$ exhibited greater abundance in our study, whereas the reverse was true in Li et al. (2019). These disparities could stem from variations in experimental conditions and instrumentation. The HOM distributions from Δ^3-carene ozonolysis showed many similarities with the corresponding α-pinene HOM under the identical conditions (Figure 1(b) &2 (a)), as was expected considering their structural similarity. However, also clear differences were

observed. Although $C_{10}H_{14,16}O_{odd}$ were the dominant monomer groups in both systems, the largest peaks in Δ^3-carene ozonolysis had a higher oxygen content ($C_{10}H_{14,16}O_9$) than those in α-pinene ozonolysis ($C_{10}H_{14,16}O_7$). Furthermore, $C_9H_{12,14}O_9$ were only abundant in the Δ^3-carene ozonolysis system. The differences in the main dimers were even more pronounced: $C_{20}H_{32}O_m$ and $C_{19}H_{30}O_n$ were the most abundant dimer groups in Δ^3-carene ozonolysis, whereas in the α-pinene system, larger $C_{19}H_{28}O_n$ signals instead of $C_{19}H_{30}O_n$ were observed.
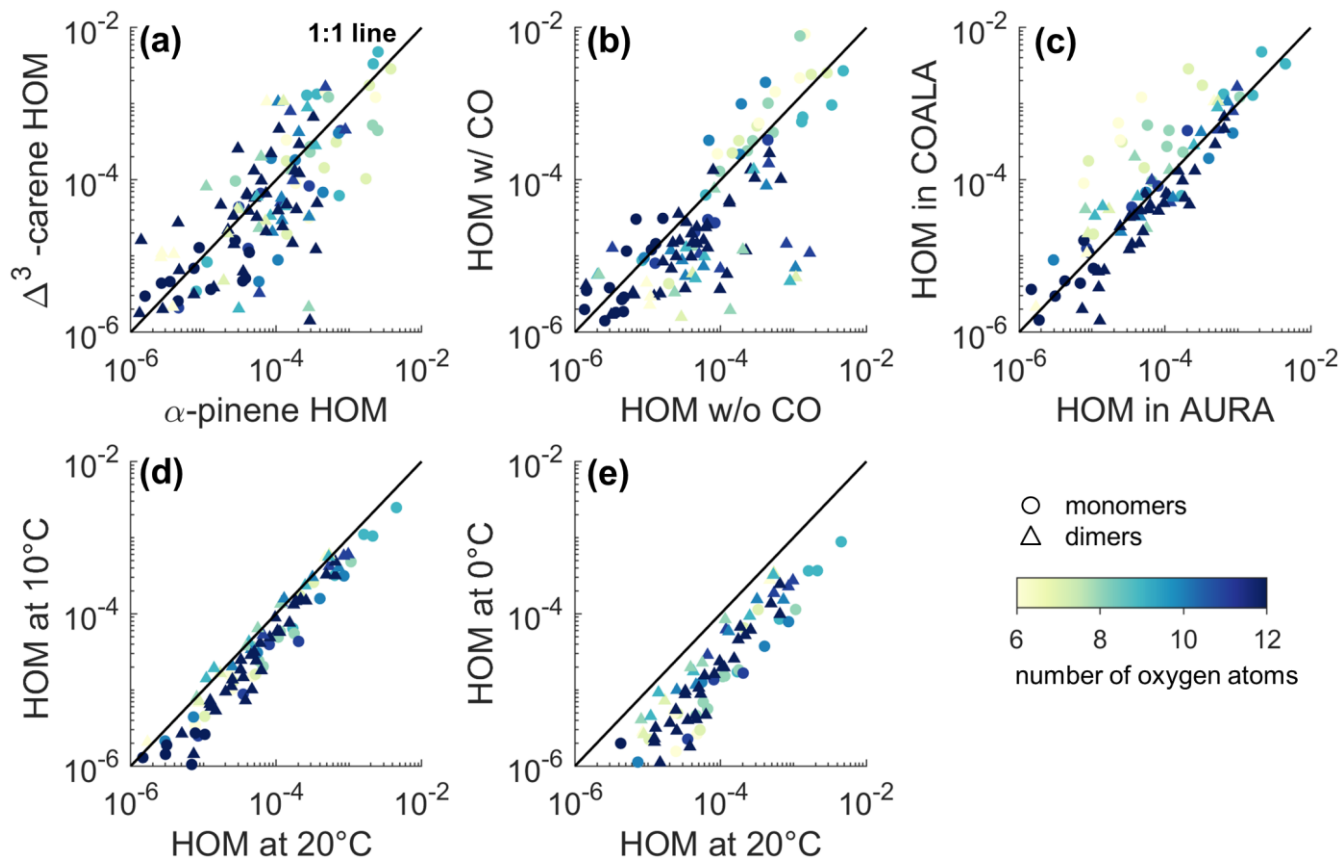
Figure 2. Scatter plots of the HOM normalized signal intensity from different experiments. Each marker corresponds to a single detected composition. The subplots depict comparisons between (a) Δ^3-carene ozonolysis (Experiment 10) and α-pinene ozonolysis (Experiment 19) in the COALA chamber, (b) Δ^3-carene ozonolysis without CO injection (Experiment 10) and with CO injection (Experiment 11) in the COALA chamber, (c) Δ^3-carene ozonolysis in COALA chamber and experiment 20B in the AURA chamber, (d) Δ^3-carene ozonolysis in the AURA chamber at 10 °C (10B) and at 20 °C (20B), and (e) Δ^3-carene ozonolysis in the AURA chamber at 0 °C (0A) and at 20 °C (20B). The colour indicates the O-atom content in the identified species, and markers distinguish monomers and dimers. The solid lines shown in all subplots are the 1:1 lines.

By grouping the detected HOM based on C-atoms and O-atoms numbers, we can see different contributions of HOM groups between the Δ^3-carene and α-pinene ozonolysis systems (Figure 3). A substantially higher fraction of C_{10} compounds and a slightly higher fraction of C_9 compounds were observed for Δ^3-carene ozonolysis, while C_8 and C_5 compounds were nearly twice as large for α-pinene ozonolysis HOM. The most significant difference within the C_9 and C_{10} groups in these two systems

was attributed to the O_9 species, which contributed more than two-fold higher to the total HOM in the Δ^3-carene system. Dam et al. (2022) also observed a larger contribution of C_9 species during the NO_3 radical oxidation of Δ^3-carene (~27%) compared to α-pinene (~10%). However, no significant C_9 signal was detected during OH oxidation of Δ^3-carene by D'Ambro et al. (2022). The reason why the larger concentration of C_9 species in Δ^3-carene ozonolysis remains unexplained based on our results. In addition, the concentration-weighted number of O-atoms for C_{10} HOM were similar; however, in the Δ^3-carene system, C_9 had a slightly higher concentration-weighted number of O-atoms, indicating the C_9 monomers were more oxidized. C_{17-20} dimers constituted approximately 33% and 21% of the total HOM from Δ^3-carene and α-pinene ozonolysis, respectively. Interestingly, $C_{19,20}$ predominated the HOM dimers from Δ^3-carene ozonolysis, while the dimer contributions from α-pinene ozonolysis exhibited a steady increasing trend as the C-atoms increased from 17 to 20. Moreover, due to the higher fractions of $O_{6,7}$ species in $C_{19,20}$ groups, the concentration-weighted numbers of O-atoms in the Δ^3-carene system were lower.
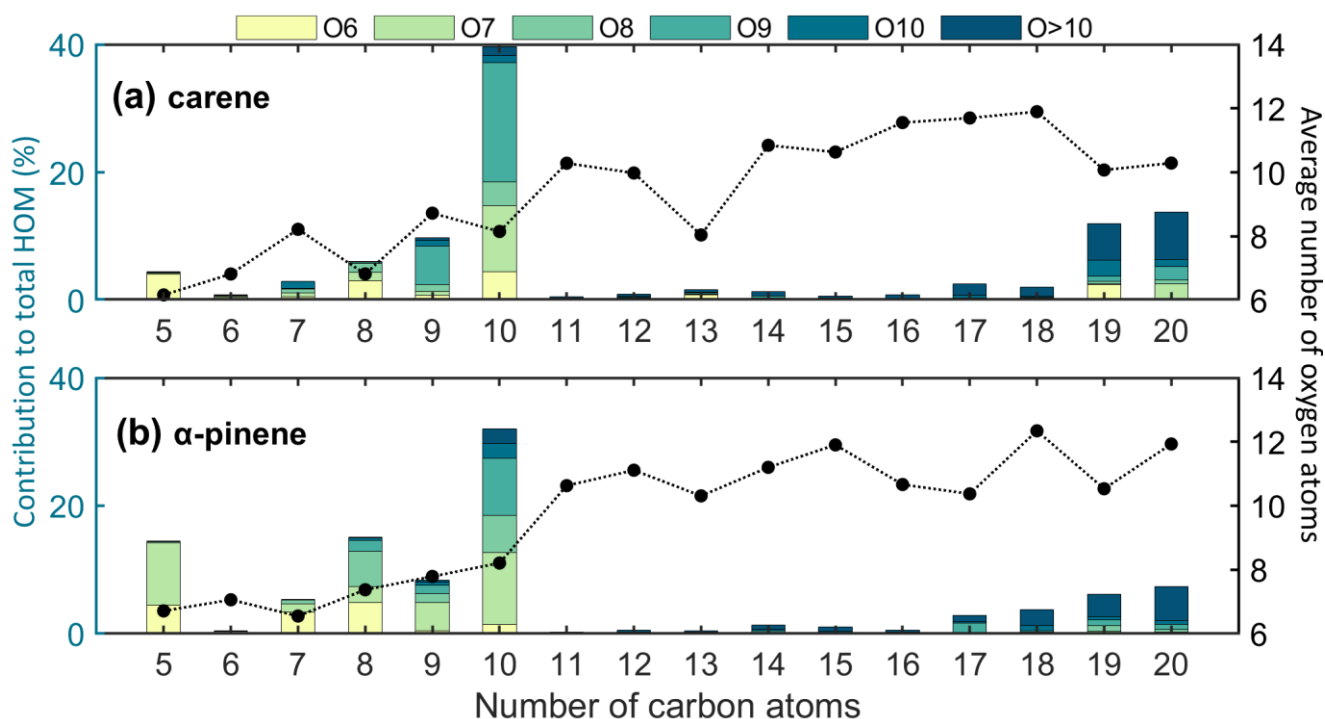
Figure 3. Fractions (left-hand y-axis) of different HOM to the total detected HOM as a function of the C-atom and O-atom number formed from (a) carene and (b) α-pinene ozonolysis in the COALA chamber under the same conditions (VOC = 20 ppb, O_3 = 30 ppb). The dots (right-hand y-axis) show the average concentration-weighted number of oxygen atoms in each HOM group with the same number of C-atoms.

Most HOM monomers shown in Figure 1(a) can be explained by the standard RO_2 chemistry described in Section 2.2. For instance, $C_{10}H_{14}O_{7,9,11}$ are likely derived from the O_3-initiated RO_2 ($C_{10}H_{15}O_{even}$) after unimolecular (R1) or bimolecular (R3, R8+9) terminations, while $C_{10}H_{16}O_{6,8,10}$ can be formed via the same termination reactions from the OH-initiated RO_2 $C_{10}H_{17}O_{odd}$. The latter can also form from $C_{10}H_{15}O_{even}$ terminating by HO_2 (R6), highlighting the complexity of determining

exact mechanisms solely from elemental composition measurements. $C_{10}H_{16}O_{7,9,11}$ HOM might be explained by $C_{10}H_{15}O_{even}$ terminating via R3 or R7 channel. In the case of the $C_{9}H_{12,14}O_{9}$ HOM which stood out in the monomer region, they have undergone a fragmentation reaction, which may be associated with an alkoxy decomposition pathway like R10. Extremely rapid RO scissions were recently shown to be highly competitive in the α-pinene ozonolysis system (Peräkylä et al., 2023), losing formaldehyde to become C_{9} radicals, though in that case they always seemingly ended up forming dimer species. The reason why C_{9} monomers were abundantly observed in only Δ^{3}-carene ozonolysis remains unclear.

For all Δ^{3}-carene ozonolysis experiments, we observed $C_{10}H_{15}O_{8,10}$ and $C_{9}H_{13}O_{10}$ as the three largest signals of radicals, consistent with the detected closed-shell HOM. Although the COALA chamber is a steady state chamber, we can examine the rates at which different species appear when we start adding reagents to the chamber. The appearance time for a species was determined when the subsequent signal change exceeded both the mean value and standard deviation of the background level. Selected time series of closed shell HOM and radicals are shown in Figure 4, and we can see that $C_{10}H_{14}O_{9}$ began to rise immediately once $C_{10}H_{15}O_{10}$ was formed, suggesting that $C_{10}H_{14}O_{9}$ was primarily formed from the unimolecular termination pathway (R1). However, $C_{9}H_{12,14}O_{9}$ and $C_{10}H_{16}O_{9}$, of which the formation process was expected to involve at least one step of $RO_{2} + RO_{2}$ reactions, started to increase ~3 min later. This reinforces our speculation on the potential formation pathways of the most abundant HOM monomers.$C_{20}H_{30,32,34}O_{x}$ dimers could originate from reactions between $C_{10}H_{15}O_{even}$ and $C_{10}H_{17}O_{odd}$, depending on the oxidant combinations. Similarly, the formation of $C_{19}H_{30}O_{n}$ and $C_{19}H_{28}O_{m}$ (m, n ≥6) dimers can be formed from combinations of the two C_{10} radicals with the $C_{9}H_{13}O_{x}$ radicals that were potentially formed via the alkoxy scissions as described above.

The relative impact of OH for HOM formation was investigated by injecting around 200 ppm CO into the COALA chamber, resulting in over 90% of OH reacting with CO instead of Δ^{3}-carene, forming a significant amount of HO_{2} in the process (Gutbrod et al., 1997). The differences in HOM formation with and without CO presence are illustrated in Figure S5(a) and Figure 2(b). Evidently, almost all dimer signals decreased significantly after CO addition, as the elevated HO_{2} level increased the competitiveness of $HO_{2} + RO_{2}$ reactions relative to $RO_{2} + RO_{2}$ reactions. However, the HOM monomers responded differently upon the CO addition (Figure S6(a)). $C_{10}H_{14}O_{odd}$ and $C_{10}H_{16}O_{odd}$ decreased, while $C_{10}H_{16}O_{even}$ increased. The latter is easily explained by increased HO_{2} termination of the O_{3}-derived RO_{2}, while the $C_{10}H_{16}O_{odd}$ decrease was expected since their major source was believed to be OH-derived RO_{2}. Interestingly, $C_{10}H_{14}O_{even}$ and $C_{9}H_{12,14}O_{even}$ monomers, of which the formation pathways were also expected to involve bimolecular reactions between RO_{2}, did not decline. One possible explanation is that $C_{10}H_{15}O_{even} + HO_{2}$ reactions yield a considerable amount of RO via R8. In contrast, no similar trends of $C_{10}H_{14}O_{even}$ and $C_{9}H_{12,14}O_{even}$ monomers were observed in the α-pinene system (Figure S6(b)). All trends observed in the α-pinene system can be explained by the decrease of OH-initiated RO_{2} and the reduced likelihood of $RO_{2} + RO_{2}$ reactions. These findings again emphasize the difference in oxidation pathways between Δ^{3}-carene and α-pinene systems.

Figure 2(c) displays the scatter diagram of the relationship between Δ^{3}-carene ozonolysis HOM observed in the AURA chamber at 20 °C and in the COALA chamber at room temperature (25 ± 1°C). HOM monomers with 9 or more O-atoms and most HOM dimers with decent signal intensities agreed very well. However, HOM monomers with 6-8 O-atoms were observed

at higher concentrations in the COALA chamber. This discrepancy could result from various factors, including differences in the experimental conditions of the two chambers, as well as variations in the configuration of the NO_3-CIMS used. Moreover, the COALA chamber spectrum was measured during the steady stage, while the data from the AURA chamber were collected at experiment time = 10 min. The HOM monomers with 6-8 O-atoms are expected to be close to semi-volatile, leading to more complex behaviour in terms of wall interactions and possible accumulation during an experiment. This topic is discussed in more detail in the next section.
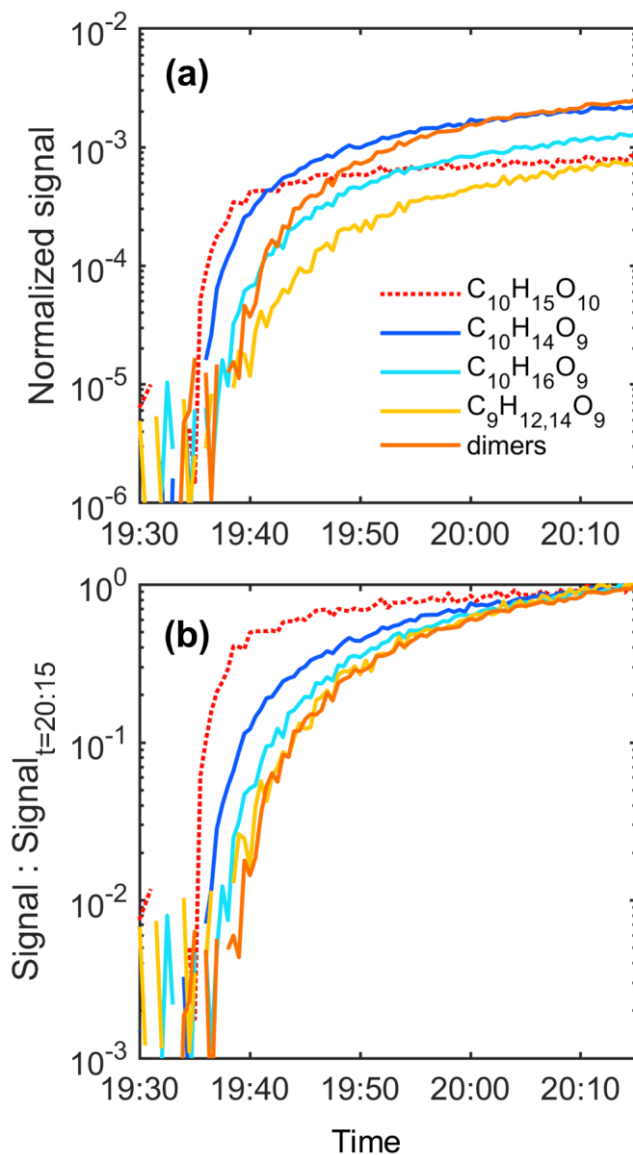
Figure 4. (a) Time series of the selected HOM and radical in experiment 10 after the injection of Δ^3-carene started. (b) The same data as in panel (a), however, each trace was normalized to its corresponding signal at 20:15 (the final data point in panel (a)) to display the relative change rate of the selected species. The red line is dashed to highlight that it is the only radical species ($C_{10}H_{15}O_{10}$)

shown in this figure. The yellow solid line represents the normalized sum of the signal intensities of $C_9H_{12,14}O_9$. Meanwhile, the red solid line illustrates the sum of the normalized signal intensities of the eight highest dimers. The time resolution of data shown in this figure is 30s.

3.2. Relative volatilities

For Δ^3-carene ozonolysis experiments conducted in the AURA chamber, a typical time series of key compounds are shown in Figure S7(b). HOM were formed via autoxidation and accumulated within the first 10 min following Δ^3-carene injection (experiment time = 0 min), but concentrations began to decrease after this due to the increasing condensation sink (CS) caused by the newly formed particles. The lifetime of HOM in the chamber was on the timescale of minutes, which meant that as long as the source (rate of Δ^3-carene oxidation) and loss (condensation onto walls or particles) changed on longer timescales, the HOM concentration could be considered to be balanced by the instantaneous source and loss terms for most of the experiment. This was at least true for the least volatile HOM, which do not accumulate in the chamber over time. The ability of HOM to condense is linked to their volatilities, with dimers generally classified as extremely low-volatility organic compounds (ELVOCs) that can irreversibly condense on particles (Peräkylä et al., 2020). Thus, we used dimer $C_{20}H_{32}O_{11}$ as a reference to probe the relative volatility of different HOM monomers compared to dimers. All other ELVOC with a similar formation pathway should behave similarly to the dimers, while more volatile products were expected to accumulate in the chamber as their removal through condensation was less efficient. Hence, in each experiment, the change in the ratio of each HOM to $C_{20}H_{32}O_{11}$ indicates the relative volatility of that molecule, though it is crucial to recognize that also differences in the formation pathways can influence the ratios.

The signal ratio of each HOM to $C_{20}H_{32}O_{11}$ ($M:C_{20}H_{32}O_{11}$, where M represents the signal intensity of HOM M) at each time point was first calculated, and then normalized by dividing it by the ratio value at experiment time=10 min. This calculated value is referred to as the 'normalized ratio' in subsequent discussions. Assuming all dimers are ELVOCs at 20 °C, the normalized ratios of the eight largest dimers exhibited a range of approximately 0.5-1.2 at experiment time = 70 min, as shown in Figure S8(b). This range provides a reference that suggests potential uncertainties in this method and indicates slightly different formation pathways for some dimers as well. For HOM monomers with 9 or more oxygen atoms, the normalized ratios ranged from around 0.9 to 4 (Figure 5(b)), comparable to the ratios of the HOM dimers, indicating that those monomers have identity condensation behaviour as dimers, but potentially with minor accumulation over time, or changes in formation pathways. However, for HOM monomers with 8 oxygen atoms e.g., $C_{10}H_{16}O_8$, the ratio was one order of magnitude higher than those for HOM with ≥ 9 oxygen atoms (e.g., $C_9H_{12}O_9$), indicating that HOM monomers with 8 oxygen atoms from Δ^3-carene ozonolysis are still to some extent semi-volatile. For HOM with 6 or 7 O-atoms, the accumulation over the experiment was considerably higher, in the order of 10-100 times more, suggesting clearly higher volatilities compared to dimers. Interestingly, the ratios of HOM with 6-8 O-atoms exhibited a significant decrease with decreasing temperature (Figure 5(b)-(d)) suggesting their lower volatilities at colder temperatures.

Peräkylä et al. (2020) evaluated the volatilities of HOM from α-pinene ozonolysis at room temperature and observed similar trends of volatilities as a function of oxygen content, although the transition from semi-volatile to low-volatility products appears to take place between O_8 to O_9 in our Δ^3-carene study, whereas their study on α-pinene ozonolysis had the transition between O_7 and O_8. The methods used were different, and our method is purely qualitative, so further work is needed to determine volatilities more quantitatively to assess if Δ^3-carene HOM indeed are slightly more volatile than α-pinene HOM with the same elemental formulas.
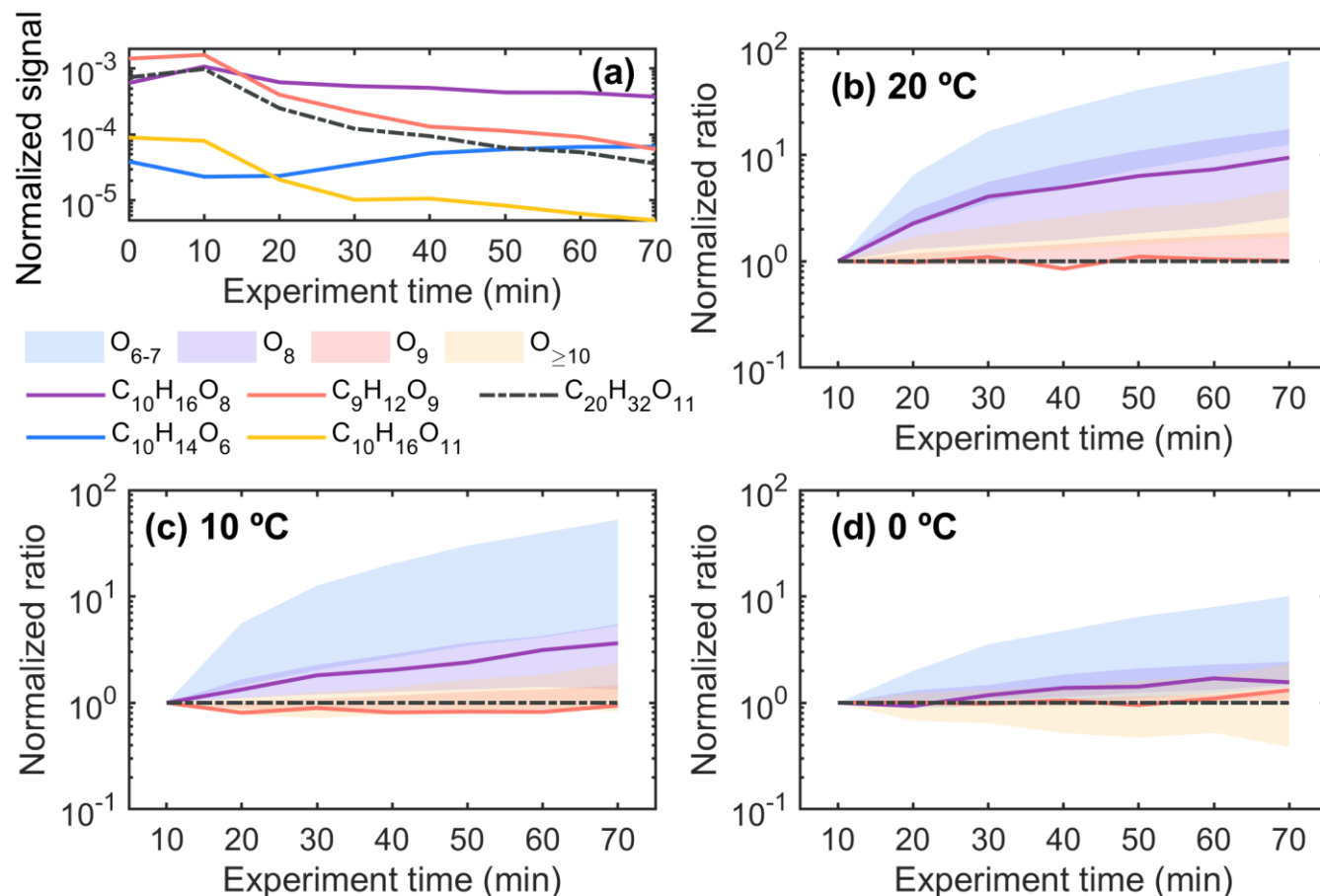
Figure 5. (a) Normalized signal intensity of the selected HOM during the 20B experiment and temporal behaviours of the ratios of different $C_{9,10}$ monomers (M) to the reference dimer ($C_{20}H_{32}O_{11}$) at (b) 20 ºC (20B), (c) 10 ºC(10B) , and (d) 0 ºC (0A) in the AURA chamber. The "normalized ratio" on the y-axis in panels (b)-(d) was determined by first calculating the ratio M:$C_{20}H_{32}O_{11}$ at each time point, which was then normalized by dividing it by the ratio value at experiment time=10 min. While absolute concentrations may differ for different species due to varying branching ratios, the normalized ratio provides the relative change of M compared to $C_{20}H_{32}O_{11}$ as a function of time. In cases where the normalized ratio is close to unity for the entire experiment, both the formation and loss rates change similarly, meaning that their condensational loss (i.e. volatility) is equal. Larger normalized ratios indicate accumulation in the chamber over time, which is likely indicative of higher volatility. The shaded areas represent the range of normalized ratios for different HOM groups.

3.3. Temperature impact on HOM formation

Temperature can strongly affect chemical reaction rates, in particular for unimolecular reactions (Rissanen et al., 2014; Kürten et al., 2015). In the AURA chamber, we performed Δ^3-carene ozonolysis experiments at three different temperatures, and the detected HOM detected are shown in Figure 6 (a)-(c). The dominant peaks in both the HOM monomer and dimer ranges remained consistent across all temperatures with $C_{10}H_{14,16}O_9$ and $C_9H_{12,14}O_9$ as the predominant HOM monomers, and $C_{19}H_{30}O_{6,10,11}$ and $C_{20}H_{32}O_{7,9,11}$ as the largest dimers. However, HOM concentrations decreased with decreasing temperature (Figure 2(d) & (e)), in part because the initial VOC oxidation slows down, but probably in much larger part due to the autoxidation process becoming slower at the colder temperatures.
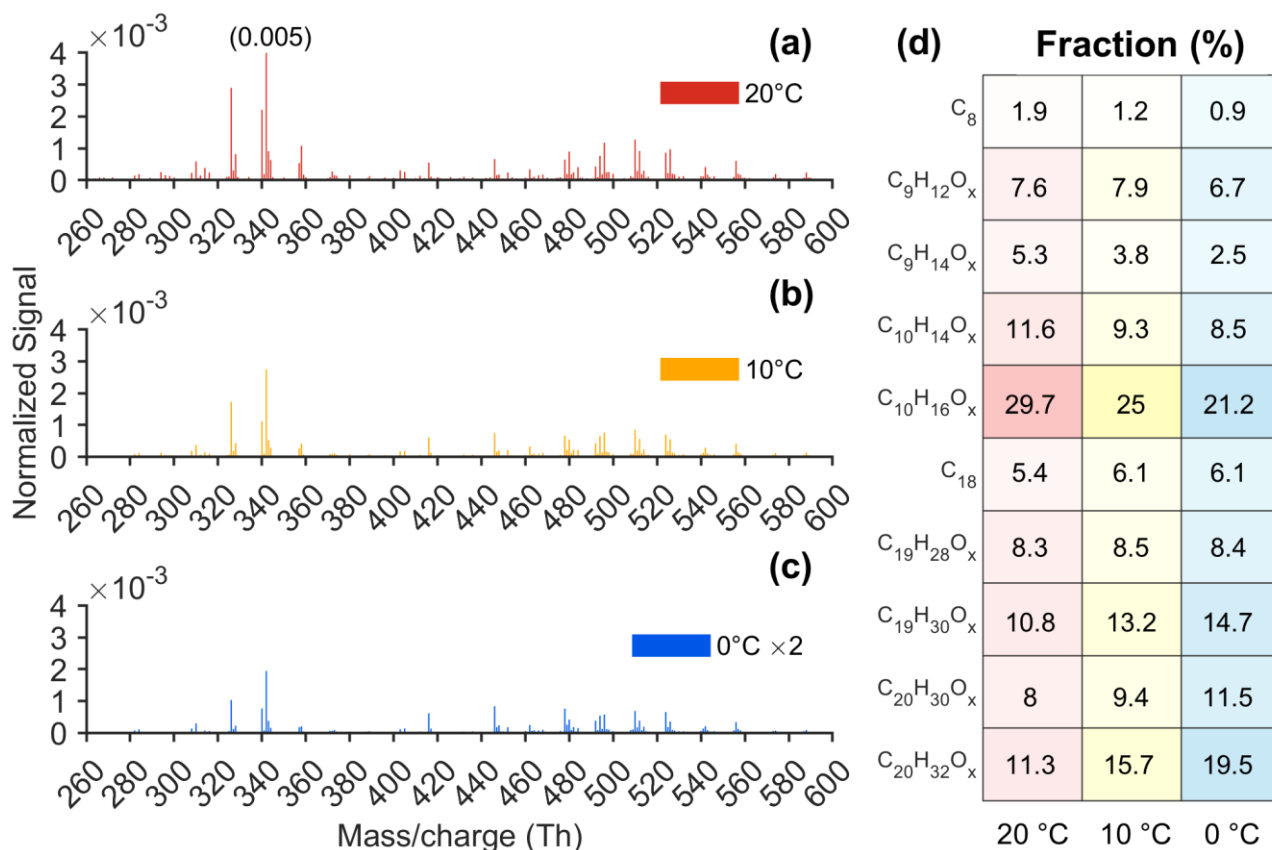
Figure 6. (a)-(c) UMR (unit-mass resolution) mass spectra from Δ^3-carene ozonolysis at 20 °C, 10 °C, and 0 °C, and **(d)** the fractions of different HOM groups (O$_X$: X $\geq$6) to the total HOM at 20 °C, 10 °C, and 0 °C in the AURA chamber. The dataset at 20 °C, 10 °C, and 0 °C is from experiment 20B, 10B, and 0A (Table S2), respectively. The signal intensities were multiplied by 2 at 0 °C in panel (c). The colour saturation in panel (d) represents the fraction, with the base colour corresponding to different temperatures shown in panels (a)-(c). All normalized signals were subtracted by the background and averaged over the period from 10 min to 20 min after Δ^3-carene injection.

Figure 6 (d) indicates quite complex changes in the yields of different HOM groups. In general, the contributions of each HOM monomer group to the total HOM decreased, while the fractions of most dimer group increased at colder temperature, resulting in the increase of HOM dimers-to-monomers ratios from 0.78 at 20°C to 1.51 at 0 °C, which indicates that the dimers decreased at a slower rate than the monomers. The slower decrease in dimers may be due to a higher formation rate or a lower loss rate. Notably, these data were collected at experiment time = 10 min when CS and wall loss for HOM were not expected to be yet significant, thus the difference of a factor of ~2 in dimers-to-monomers ratios could be primarily due to the differences in their formation. A plausible hypothesis is that a colder temperature may favour the dimerization pathway of $RO_2 + RO_2$, allowing the formed complex of two RO to remain bound for a longer time (R4). Consequently, the probability of $RO_2 + RO_2$ reactions forming dimers was higher, leading to a less significant decrease in the concentrations of dimers compared to monomers. Simon et al. (2020) also observed an increase in the dimers-to-monomers as temperatures decreased within the temperature range studied for α-pinene ozonolysis. In contrast, Quéléver et al. (2019) reported that HOM dimers from α-pinene ozonolysis decreased at a faster rate than monomers when temperatures dropped. Those experiments in Quéléver et al. (2019) were performed at higher loadings, which might explain the difference, but it is also possible that the dimer yields are different for the two systems under different temperatures, as the dimer formation mechanism is highly structure-dependent (Hasan et al., 2020; Valiev et al., 2019; Daub et al., 2022a; Daub et al., 2022b; Hasan et al., 2021). Additionally, variations in experimental (e.g., reagents concentrations) and instrumental settings (e.g., voltages) between the two studies represent a notable source of uncertainty that could contribute to these differences. It is also important to note that the colder sample air may cause some changes to the CIMS response, and we cannot rule out the influence of this. However, by the time the air enters the mass spectrometer itself, the air has very likely reached very close to room temperature, given the addition of a room-temperature sheath flow in the CI inlet, and thus any dramatic changes in e.g. mass-dependent transmission is not expected.

In order to estimate HOM molar yields from the Δ^3-carene ozonolysis, we need to estimate the loss rates of the HOM. For species with some semi-volatile character, this was not possible, and therefore our yield calculations are limited to HOM monomers with 9 or more O-atoms and all HOM dimers with O-atoms ≥ 6 (hereafter referred to as "$HOM_{O\geq9}$"). Note that the yield of $HOM_{O\geq9}$ should be slightly lower than the total HOM yield, as we do not include all HOM. The majority of the data from Δ^3-carene ozonolysis experiments conducted in the COALA chamber can be explained by $HOM_{O\geq9}$ yields of 3 to 6% (Figure S9). Although as noted in Section S2, the absolute calibration of the NO_3-CIMS comes with a large uncertainty, we can compare the resulting yield to that of α-pinene ozonolysis in the COALA chamber under identical conditions. From our experiments, we estimate a $HOM_{O\geq9}$ yield of 2-4 % for α-pinene ozonolysis, which is in good agreement with previous studies (Jokinen et al., 2015; Ehn et al., 2014). Thus, our results suggest that the Δ^3-carene ozonolysis yields around 1.5-folder higher HOM concentrations than α-pinene under identical conditions. We also estimated the $HOM_{O\geq9}$ yield for all the Δ^3-carene ozonolysis experiments performed in the AURA chamber (Figure 7), even though the calculation becomes slightly more complicated (Section S2). We found that the $HOM_{O\geq9}$ yield at 20 °C was ~4% for 20A and ~3 % for 20B, which was within the range estimated for the experiments in the COALA chamber. However, the yields for the four experiments at 10 °C differ significantly, ranging from 0.2 to 2.6%. The large uncertainties of the yields at 10 °C might be attributed to the different

settings of the NO₃-CIMS described in Section S1. Examining only the experiments conducted with the same instrumental settings (20B, 10B and 0A, blue circles in Figure 7), there is a clear decrease from around 3 % to below 1 % in the $HOM_{O \geq 9}$

380 yields when temperature dropped from 20 °C to 0 °C. This decrease is slightly larger than that observed for α-pinene ozonolysis by Simon et al. (2020) in the CLOUD chamber, in which the total HOM yields declined from 6.2% at 25 °C to 4.7% at 5 °C. However, Quéléver et al. (2019) reported a much larger drop (around 50-fold) in the α-pinene system upon a temperature decrease from 20 °C to 0 °C. Some of these differences may arise from the different conditions of the experiments, in particular the VOC loadings used. At higher loadings, the RO_2 lifetime is shorter, and a change in RO_2 H-shift rates may have a more

385 dramatic impact when the competing reactions are faster. We hope more studies will focus on the temperature dependent HOM yields in order to better understand these reported differences. We also again emphasize the large uncertainties (at least a factor 3) in our molar yield estimations, though the relative difference between the yields from Δ^3-carene ozonolysis and α-pinene ozonolysis (using the same conditions and instruments) is expected to be much smaller.

390
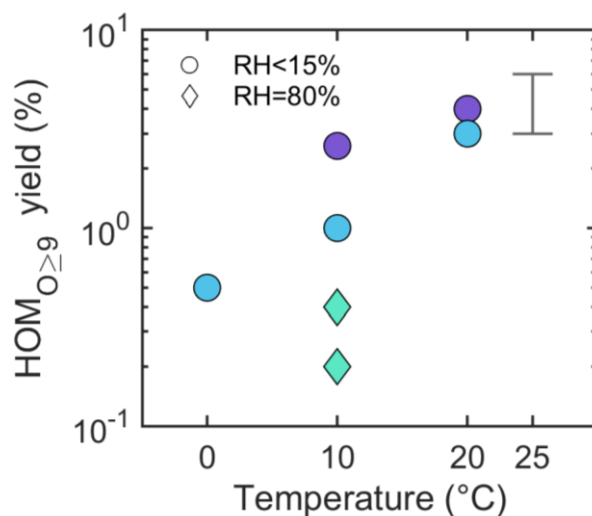
Figure 7. Estimated $HOM_{O \geq 9}$ (the sum of HOM monomers with no less than 9 O-atoms and all HOM dimers (O-atoms ≥ 6)) molar yields in the AURA chamber at different temperatures. Colors represent different operational conditions of the NO₃-CIMS, which correspond to the colors in Figure S2. Error bar marks the yield range estimated from Δ^3-carene ozonolysis experiments in the COALA chamber at room temperature.

395 **3.4. RH impact on HOM formation**

Previous studies on the yield and distribution of HOM have found them to not be affected significantly by RH (Li et al., 2019; Peräkylä et al., 2020), indicating that HOM formation pathways are largely water-independent. We performed two experiments (10D and 10E) in the AURA chamber under high RH condition (RH = 80%) with two different VOC loadings (Table S2) which could be used to check the RH impact on HOM formation. The mass spectra indicated that the main peaks of HOM

were similar under both dry and humid conditions (Figure S10(a)-(c)), although the NO_3-CIMS was also sensitive to water clusters, the detection precision of HOM with the same m/z as the water clusters (Figure S10(b)-(c)) was slightly hampered. However, the absolute signal intensities of most HOM monomers and dimers at RH = 80 % were approximately 7 times lower than that with the similar VOC and O_3 under dry condition (Figure S10(d)). Unfortunately, it is difficult to attribute this dramatic drop solely to the elevated RH, as the instrument settings were different between these two experiments (10B and 10 D in Table S2), although we applied a correction factor to reduce the influence of the different settings on the HOM detection. High RH can increase the CS for HOM, thereby reducing their concentrations, but this effect is expected to be quite low in this case. We observed that the HOM signal increased by a factor of ~3 when we injected twice the amount of Δ^3-carene into the chamber at RH = 80 %, and the rise of HOM dimer signals was even more pronounced than that of monomers (Figure S10(e)). Overall, the quality of our data for this comparison is poor, and we cannot state with certainty whether the RH actually had an impact on the HOM formation pathways, but we mention these results here nevertheless, hoping to prompt further studies to quantify the RH impact on HOM formation from Δ^3-carene ozonolysis.

3.5. HOM simulation by ADCHAM

A modified peroxy radical autoxidation mechanism was developed specifically to be able to replicate the observed HOM formation during the AURA and COALA Δ^3-carene ozonolysis experiments. In Figure 8 we compare the modelled and measured HOM concentrations during the COALA experiments where 200 ppm CO was added after approximately 5 hours. The model is able to predict the observed absolute concentrations of HOM monomers and dimers and how the general patterns in the HOM observations change upon CO addition. Unimolecular termination (R1) of $C_{10}H_{15}O_8$ may explain why the $C_{10}H_{14}O_7$ concentration do not decrease substantially during the CO addition. However, the model cannot explain why the $C_{10}H_{16}O_7$ signal does not decrease appreciable during the CO addition. The model verifies that increasing HO_2 concentration upon CO addition can explain the observed decreasing concentrations of $C_{10}H_{14,16}O_9$, $C_9H_{12,14}O_9$ and HOM dimers, and increasing concentrations of $C_{10}H_{16}O_{8,10}$ and $C_9H_{14}O_{10}$ (Figure S11). The substantial decrease of $C_{10}H_{14,16}O_9$, but moderate increase of $C_{10}H_{16}O_{10}$, upon CO addition is captured by the model if assuming that only a minor fraction (~25%) of the $C_{10}H_{15}O_{10}$ + HO_2 reactions result in $C_{10}H_{16}O_{10}$ products via R6. For all other PRAM RO_2+HO_2 reactions, the ROOH formation via R6 was considered the only production pathway.

The absolute $HOM_{O\geq9}$ yields and their temperature dependences agree reasonably well with the observations in AURA (Figure 9). $HOM_{O\geq9}$ account for <5%, 5-9% and 12-15% of the modelled total SOA mass in AURA at 0, 10 and 20 °C, respectively (Figure S12). The $HOM_{O\geq9}$ SOA fraction depends both on the temperature and the VOC loading. The model also demonstrates how the HOM yields become higher and less sensitive to the temperature in the chamber when the VOC concentration decreases to more typical atmospheric levels (<1 ppbv), as observed in previous CLOUD chamber experiments(Simon et al., 2020; Nie et al., 2023).
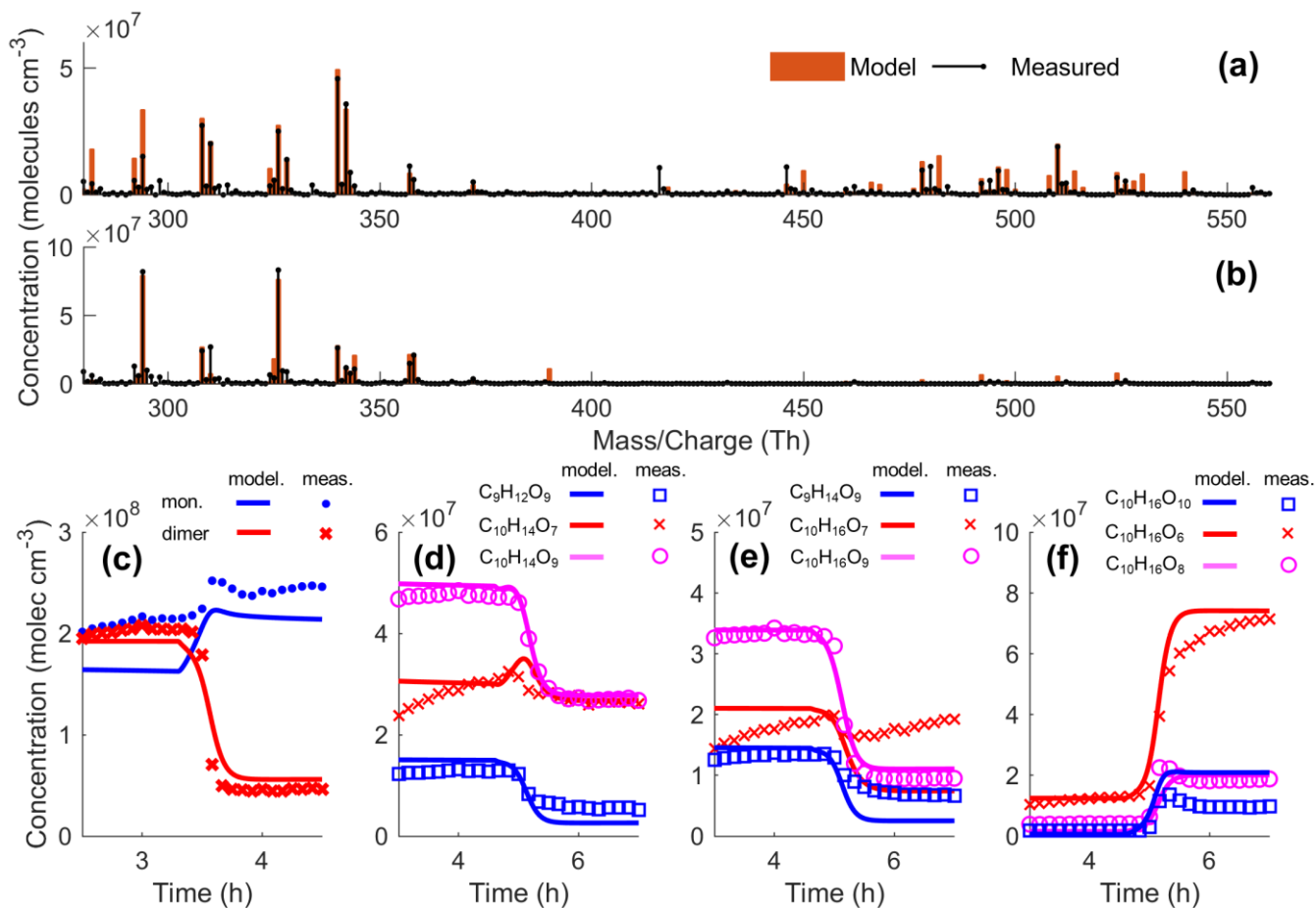
Figure 8. Evaluation of modelled HOM concentrations during an ozonolysis Δ³-carene experiment in COALA (Experiment 10: VOC = 20 ppb, O_3 = 30 ppb), with addition of CO (Experiment 11: VOC = 20 ppb, O_3 = 30 ppb, CO= 200 ppm). Panel (a) shows the modelled and measured mass spectrum before CO addition and panel (b) after CO addition. Panel (c) shows the modelled and measured total HOM monomer (Mass/charge 312-384 Th) and HOM dimer (Mass/charge 385-600 Th) concentrations and panels (d), (e) and (f) shows the concentrations of the major closed shell HOM monomer species. For panels (c)-(f), CO was injected at time=~5 h.
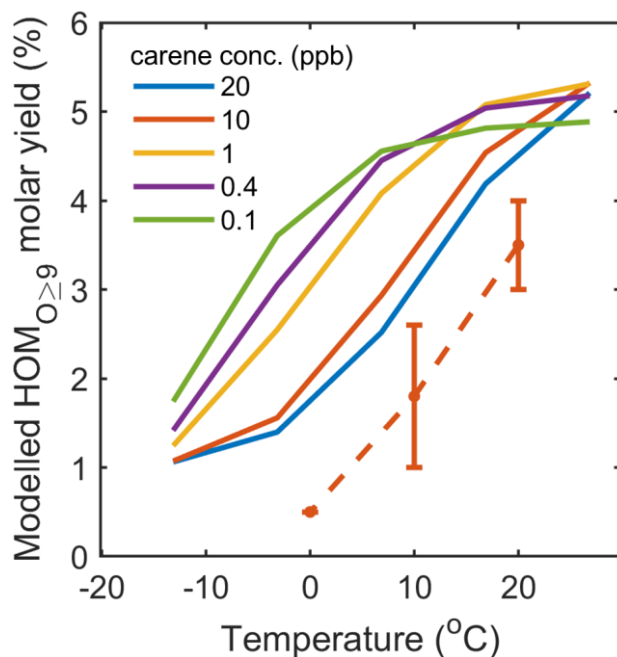
Figure 9. Modelled HOM$_{O\geq9}$ molar yields for conditions with different fixed Δ^3-carene concentrations and an ozone concentration of 30 ppb. The dashed line with error bars represents measured HOM$_{O\geq9}$ molar yields with 10 ppb initial Δ^3-carene under dry conditions. At low (atmospheric relevant) Δ^3-carene concentrations of ≤1 ppb the HOM$_{O\geq9}$ yields decrease with <25 % between +25 °C and 5 °C, while at Δ^3-carene concentrations ≥10 ppb the HOM$_{O\geq9}$ yields decrease with >50%.

4. Conclusions

HOM formation from O$_3$-initiated Δ^3-carene oxidation was investigated in two simulation chambers. Our findings reveal that ozonolysis of Δ_3-carene yields HOM monomers (C$_{7-10}$H$_{10-18}$O$_{6-14}$) and dimers (C$_{17-20}$H$_{24-34}$O$_{6-18}$). The detected HOM could mostly be explained by RO$_2$ from O$_3$-initiated (C$_{10}$H$_{15}$O$_{even}$) or OH-initiated (C$_{10}$H$_{17}$O$_{odd}$) oxidation followed by autoxidation and different termination reactions. Our study also identified that HOM monomers with 9 or more O-atoms and all dimers typically condense onto particles irreversibly. However, HOM monomers with 6-8 O-atoms behaved more similarly to semi-volatile organic species, maintaining a noticeable gas phase concentration. The HOM$_{O\geq9}$ yield at room temperature was estimated to be higher than that of α-pinene ozonolysis under the same conditions, with our best estimate being in the range 3-6 %.

We observed that HOM concentrations decreased considerably at lower temperatures. This observation is consistent with previous studies on α-pinene ozonolysis (Quéléver et al., 2019; Simon et al., 2020) , though the extent of the decrease varies considerably. The ADCHAM model, featuring a modified peroxy radical autoxidation mechanism, predicted the decrease observed in our study. However, further research is warranted to understand the causes of discrepancies observed across different studies. In addition, our study found that the HOM spectra were similar at three different temperatures (20, 10 and 0

°C), and were dominated by $C_{10}H_{14,16}O_9$ and $C_9H_{12,14}O_9$ in the monomer range and $C_{19}H_{30}O_{6,10,11}$ and $C_{20}H_{32}O_{7,9,11}$ in the dimer range, respectively. However, all dimers decreased at a slower rate than monomers, resulting in an increasing HOM dimers-to-monomers ratio from 0.78 to 1.51 when the temperatures decreased from 20 °C to 0 °C, which aligns with the results reported by Simon et al. (2020) for α-pinene ozonolysis, but contrasts with the findings of Quéléver et al. (2019). The ADCHAM model managed to replicate the HOM formation, with the simulated composition, yield and temperature dependence all agreeing reasonably well with our observations. We also found a sharp decrease in HOM concentrations at high RH (80%), but due to large instrumental uncertainty during the high RH experiments, further work is required to verify the validity of this observation.

Taken together, our experimental results provide valuable insights into the Δ^3-carene ozonolysis process in the atmosphere. The characterization of HOM oxidation products and estimation of yield help to further elucidate their potential impact on SOA formation. Additionally, the comparison between the results of Δ^3-carene and α-pinene ozonolysis highlights the influence of different monoterpene precursors on the formation, distribution, and properties of HOM, consequently affecting the properties of SOA. Thus, current models that group all monoterpenes together and represent them by α-pinene may lead to inaccuracies in the predicted SOA concentrations and their ultimate impact on climate.

Data availability. Data is available upon request by contacting the corresponding authors.

Author Contributions. The experiments were conducted by YL, DT, EMI, JTS, LL, and MP. YL analysed the NO_3-CIMS and PTR-TOF data. DT, EMI, JTS, LL, and MP performed analysis of data from particle phase. PR conducted the ADCHAM model simulation. YL, DT, EMI, JTS, PR, LL, MP, PR, HBP, MH, MB, MG and ME participated in discussion of the results. YL prepared the original draft with larger contributions from PR. All authors contributed to comment on the manuscript.

Competing interests. The authors declare that they have no conflict of interest.

Acknowledgments. This research received support from the European Commission (Horizon 2020, ATMO-ACCESS grant no. 101008004), the Academy of Finland (grant nos. 317380 and 320094), Swedish Research Council VR (project no. 2019-05006), Swedish Research Council FORMAS (project no. 2018-01745), Lund University's strategic research area MERGE, the Danish National Research Foundation (DNRF172) and the China Scholarship Council (grant no. 201906220191) for YL. MH and LL were supported by Swedish Research Council (grant no. 2018–04430). The AURA chamber is funded by the Danish Agency for Higher Education and Science (ACTRIS-DK infrastructure grant). We also acknowledge funding from The Independent Research Fund Denmark (grants nos. 8021-00355B and 0136-00345B).

References

Aschmann, S. M., Atkinson, R., and Arey, J.: Products of reaction of OH radicals with α-pinene, Journal of Geophysical Research: Atmospheres, 107, ACH 6-1-ACH 6-7, 2002.

Atkinson, R. and Arey, J.: Atmospheric Degradation of Volatile Organic Compounds, Chemical Reviews, 103, 4605-4638, 10.1021/cr0206420, 2003.

Atkinson, R., Baulch, D., Cox, R., Hampson Jr, R., Kerr, J., and Troe, J.: Evaluated kinetic and photochemical data for atmospheric chemistry: Supplement IV. IUPAC subcommittee on gas kinetic data evaluation for atmospheric chemistry, Atmospheric Chemistry and Physics, 21, 1125-1568, 1992.

Bäck, J., Aalto, J., Henriksson, M., Hakola, H., He, Q., and Boy, M.: Chemodiversity of a Scots pine stand and implications for terpene air concentrations, Biogeosciences, 9, 689-702, 10.5194/bg-9-689-2012, 2012.

Baptista, L., Francisco, L. F., Dias, J. F., da Silva, E. C., dos Santos, C. V. F., de Mendonça, F. S. G., and Arbilla, G.: Theoretical study of Δ-3-(+)-carene oxidation, Physical Chemistry Chemical Physics, 16, 19376-19385, 2014.

Berndt, T., Böge, O., and Stratmann, F.: Gas-phase ozonolysis of α-pinene: gaseous products and particle formation, Atmospheric Environment, 37, 3933-3945, 10.1016/s1352-2310(03)00501-6, 2003.

Bianchi, F., Kurtén, T., Riva, M., Mohr, C., Rissanen, M. P., Roldin, P., Berndt, T., Crounse, J. D., Wennberg, P. O., and Mentel, T. F.: Highly oxygenated organic molecules (HOM) from gas-phase autoxidation involving peroxy radicals: A key contributor to atmospheric aerosol, Chemical Reviews, 119, 3472-3509, 2019.

Bianchi, F., Tröstl, J., Junninen, H., Frege, C., Henne, S., Hoyle, C. R., Molteni, U., Herrmann, E., Adamov, A., Bukowiecki, N., Chen, X., Duplissy, J., Gysel, M., Hutterli, M., Kangasluoma, J., Kontkanen, J., Kürten, A., Manninen, H. E., Münch, S., Peräkylä, O., Petäjä, T., Rondo, L., Williamson, C., Weingartner, E., Curtius, J., Worsnop, D. R., Kulmala, M., Dommen, J., and Baltensperger, U.: New particle formation in the free troposphere: A question of chemistry and timing, Science, 352, 1109-1112, 10.1126/science.aad5456, 2016.

Boy, M., Mogensen, D., Smolander, S., Zhou, L., Nieminen, T., Paasonen, P., Plass-Dülmer, C., Sipilä, M., Petäjä, T., Mauldin, L., Berresheim, H., and Kulmala, M.: Oxidation of SO2 by stabilized Criegee intermediate (sCI) radicals as a crucial source for atmospheric sulfuric acid concentrations, Atmospheric Chemistry and Phyics, 13, 3865-3879, 10.5194/acp-13-3865-2013, 2013.

Cohen, A. J., Brauer, M., Burnett, R., Anderson, H. R., Frostad, J., Estep, K., Balakrishnan, K., Brunekreef, B., Dandona, L., and Dandona, R.: Estimates and 25-year trends of the global burden of disease attributable to ambient air pollution: an analysis of data from the Global Burden of Diseases Study 2015, The lancet, 389, 1907-1918, 2017.

D'Ambro, E. L., Hyttinen, N., Moller, K. H., Iyer, S., Otkjaer, R. V., Bell, D. M., Liu, J., Lopez-Hilfiker, F. D., Schobesberger, S., Shilling, J. E., Zelenyuk, A., Kjaergaard, H. G., Thornton, J. A., and Kurten, T.: Pathways to Highly Oxidized Products in the Delta3-Carene + OH System, Environmental Science & Technology, 56, 2213-2224, 10.1021/acs.est.1c06949, 2022.

Dam, M., Draper, D. C., Marsavin, A., Fry, J. L., and Smith, J. N.: Observations of gas-phase products from the nitrate-radical-initiated oxidation of four monoterpenes, Atmospheric Chemistry and Phyics, 22, 9017-9031, 10.5194/acp-22-9017-2022, 2022.

Daub, C. D., Valiev, R., Salo, V.-T., Zakai, I., Gerber, R. B., and Kurtén, T.: Computed Pre-reactive Complex Association Lifetimes Explain Trends in Experimental Reaction Rates for Peroxy Radical Recombinations, ACS Earth and Space Chemistry, 6, 2446-2452, 10.1021/acsearthspacechem.2c00159, 2022a.

Daub, C. D., Zakai, I., Valiev, R., Salo, V.-T., Gerber, R. B., and Kurtén, T.: Energy transfer, pre-reactive complex formation and recombination reactions during the collision of peroxy radicals, Physical Chemistry Chemical Physics, 24, 10033-10043, 2022b.

Day, D. A., Fry, J. L., Kang, H. G., Krechmer, J. E., Ayres, B. R., Keehan, N. I., Thompson, S. L., Hu, W., Campuzano-Jost, P., Schroder, J. C., Stark, H., DeVault, M. P., Ziemann, P. J., Zarzana, K. J., Wild, R. J., Dubè, W. P., Brown, S. S., and Jimenez, J. L.: Secondary Organic Aerosol Mass Yields from NO3 Oxidation of α-Pinene and Δ-Carene: Effect of RO2 Radical Fate, The Journal of Physical Chemistry A, 126, 7309-7330, 10.1021/acs.jpca.2c04419, 2022.

Draper, D. C., Myllys, N., Hyttinen, N., Møller, K. H., Kjaergaard, H. G., Fry, J. L., Smith, J. N., and Kurtén, T.: Formation of Highly Oxidized Molecules from NO3 Radical Initiated Oxidation of Δ-3-Carene: A Mechanistic Study, ACS Earth and Space Chemistry, 3, 1460-1470, 10.1021/acsearthspacechem.9b00143, 2019.

Ehn, M., Thornton, J. A., Kleist, E., Sipilä, M., Junninen, H., Pullinen, I., Springer, M., Rubach, F., Tillmann, R., and Lee, B.: A large source of low-volatility secondary organic aerosol, Nature, 506, 476-479, 2014.

Fry, J. L., Draper, D. C., Barsanti, K. C., Smith, J. N., Ortega, J., Winkler, P. M., Lawler, M. J., Brown, S. S., Edwards, P. M., Cohen, R. C., and Lee, L.: Secondary Organic Aerosol Formation and Organic Nitrate Yield from NO3 Oxidation of Biogenic Hydrocarbons, Environmental Science & Technology, 48, 11944-11953, 10.1021/es502204x, 2014.

Fry, J. L., Draper, D. C., Zarzana, K. J., Campuzano-Jost, P., Day, D. A., Jimenez, J. L., Brown, S. S., Cohen, R. C., Kaser, L., Hansel, A., Cappellin, L., Karl, T., Hodzic Roux, A., Turnipseed, A., Cantrell, C., Lefer, B. L., and Grossberg, N.: Observations of gas- and aerosol-phase organic nitrates at BEACHON-RoMBAS 2011, Atmospheric Chemistry and Phyics, 13, 8585-8605, 10.5194/acp-13-8585-2013, 2013.

Geron, C., Rasmussen, R., R. Arnts, R., and Guenther, A.: A review and synthesis of monoterpene speciation from forests in the United States, Atmospheric Environment, 34, 1761-1781, https://doi.org/10.1016/S1352-2310(99)00364-7, 2000.

Glasius, M., Lahaniati, M., Calogirou, A., Di Bella, D., Jensen, N. R., Hjorth, J., Kotzias, D., and Larsen, B. R.: Carboxylic Acids in Secondary Aerosols from Oxidation of Cyclic Monoterpenes by Ozone, Environmental Science & Technology, 34, 1001-1010, 10.1021/es990445r, 2000.

545 Griffin, R. J., Cocker III, D. R., Flagan, R. C., and Seinfeld, J. H.: Organic aerosol formation from the oxidation of biogenic hydrocarbons, Journal of Geophysical Research: Atmospheres, 104, 3555-3567, 1999.

Groß, C. B. M., Dillon, T. J., Schuster, G., Lelieveld, J., and Crowley, J. N.: Direct Kinetic Study of OH and O3 Formation in the Reaction of CH3C(O)O2 with HO2, The Journal of Physical Chemistry A, 118, 974-985, 10.1021/jp412380z, 2014.

Guenther, A. B., Jiang, X., Heald, C. L., Sakulyanontvittaya, T., Duhl, T., Emmons, L. K., and Wang, X.: The Model of Emissions of Gases and Aerosols from Nature version 2.1 (MEGAN2.1): an extended and updated framework for modeling biogenic emissions, Geoscientific

550 Model Development, 5, 1471-1492, 10.5194/gmd-5-1471-2012, 2012.

Gutbrod, R., Meyer, S., Rahman, M. M., and Schindler, R. N.: On the use of CO as scavenger for OH radicals in the ozonolysis of simple alkenes and isoprene, International Journal of Chemical Kinetics, 29, 717-723, 1997.

Hallquist, M., Wängberg, I., Ljungström, E., Barnes, I., and Becker, K.-H.: Aerosol and Product Yields from NO3 Radical-Initiated Oxidation of Selected Monoterpenes, Environmental Science & Technology, 33, 553-559, 10.1021/es980292s, 1999.

555 Hallquist, M., Wenger, J. C., Baltensperger, U., Rudich, Y., Simpson, D., Claeys, M., Dommen, J., Donahue, N. M., George, C., Goldstein, A. H., Hamilton, J. F., Herrmann, H., Hoffmann, T., Iinuma, Y., Jang, M., Jenkin, M. E., Jimenez, J. L., Kiendler-Scharr, A., Maenhaut, W., McFiggans, G., Mentel, T. F., Monod, A., Prévôt, A. S. H., Seinfeld, J. H., Surratt, J. D., Szmigielski, R., and Wildt, J.: The formation, properties and impact of secondary organic aerosol: current and emerging issues, Atmospheric Chemistry and Physics, 9, 5155-5236, 10.5194/acp-9-5155-2009, 2009.

560 Hantschke, L., Novelli, A., Bohn, B., Cho, C., Reimer, D., Rohrer, F., Tillmann, R., Glowania, M., Hofzumahaus, A., Kiendler-Scharr, A., Wahner, A., and Fuchs, H.: Atmospheric photooxidation and ozonolysis of Δ3-carene and 3-caronaldehyde: rate constants and product yields, Atmospheric Chemistry and Physics, 21, 12665-12685, 10.5194/acp-21-12665-2021, 2021.

Hasan, G., Valiev, R. R., Salo, V.-T., and Kurtén, T.: Computational Investigation of the Formation of Peroxide (ROOR) Accretion Products in the OH- and NO3-Initiated Oxidation of α-Pinene, The Journal of Physical Chemistry A, 125, 10632-10639, 10.1021/acs.jpca.1c08969,

565 2021.

Hasan, G., Salo, V.-T., Valiev, R. R., Kubečka, J., and Kurtén, T.: Comparing Reaction Routes for 3(RO···OR′) Intermediates Formed in Peroxy Radical Self- and Cross-Reactions, The Journal of Physical Chemistry A, 124, 8305-8320, 10.1021/acs.jpca.0c05960, 2020.

Hasson, A. S., Kuwata, K. T., Arroyo, M. C., and Petersen, E. B.: Theoretical studies of the reaction of hydroperoxy radicals (HO2) with ethyl peroxy (CH3CH2O2), acetyl peroxy (CH3C(O)O2), and acetonyl peroxy (CH3C(O)CH2O2) radicals, Journal of Photochemistry and

570 Photobiology A: Chemistry, 176, 218-230, https://doi.org/10.1016/j.jphotochem.2005.08.012, 2005.

Hoffmann, T., Odum, J. R., Bowman, F., Collins, D., Klockow, D., Flagan, R. C., and Seinfeld, J. H.: Formation of Organic Aerosols from the Oxidation of Biogenic Hydrocarbons, Journal of Atmospheric Chemistry, 26, 189-222, 10.1023/A:1005734301837, 1997.

Jimenez, J. L., Canagaratna, M. R., Donahue, N. M., Prevot, A. S. H., Zhang, Q., Kroll, J. H., DeCarlo, P. F., Allan, J. D., Coe, H., Ng, N. L., Aiken, A. C., Docherty, K. S., Ulbrich, I. M., Grieshop, A. P., Robinson, A. L., Duplissy, J., Smith, J. D., Wilson, K. R., Lanz, V. A.,

575 Hueglin, C., Sun, Y. L., Tian, J., Laaksonen, A., Raatikainen, T., Rautiainen, J., Vaattovaara, P., Ehn, M., Kulmala, M., Tomlinson, J. M., Collins, D. R., Cubison, M. J., null, n., Dunlea, J., Huffman, J. A., Onasch, T. B., Alfarra, M. R., Williams, P. I., Bower, K., Kondo, Y., Schneider, J., Drewnick, F., Borrmann, S., Weimer, S., Demerjian, K., Salcedo, D., Cottrell, L., Griffin, R., Takami, A., Miyoshi, T., Hatakeyama, S., Shimono, A., Sun, J. Y., Zhang, Y. M., Dzepina, K., Kimmel, J. R., Sueper, D., Jayne, J. T., Herndon, S. C., Trimborn, A. M., Williams, L. R., Wood, E. C., Middlebrook, A. M., Kolb, C. E., Baltensperger, U., and Worsnop, D. R.: Evolution of Organic Aerosols

580 in the Atmosphere, Science, 326, 1525-1529, 10.1126/science.1180353, 2009.

Jokinen, T., Berndt, T., Makkonen, R., Kerminen, V. M., Junninen, H., Paasonen, P., Stratmann, F., Herrmann, H., Guenther, A. B., Worsnop, D. R., Kulmala, M., Ehn, M., and Sipila, M.: Production of extremely low volatile organic compounds from biogenic emissions: Measured yields and atmospheric implications, The Proceedings of the National Academy of Sciences, 112, 7123-7128, 10.1073/pnas.1423977112, 2015.

585 Kim, S., Wolfe, G. M., Mauldin, L., Cantrell, C., Guenther, A., Karl, T., Turnipseed, A., Greenberg, J., Hall, S. R., Ullmann, K., Apel, E., Hornbrook, R., Kajii, Y., Nakashima, Y., Keutsch, F. N., DiGangi, J. P., Henry, S. B., Kaser, L., Schnitzhofer, R., Graus, M., Hansel, A., Zheng, W., and Flocke, F. F.: Evaluation of HOx sources and cycling using measurement-constrained model calculations in a 2-methyl-3-butene-2-ol (MBO) and monoterpene (MT) dominated ecosystem, Atmospheric Chemistry and Phyics, 13, 2031-2044, 10.5194/acp-13-2031-2013, 2013.

590 Kristensen, K., Jensen, L. N., Quéléver, L. L. J., Christiansen, S., Rosati, B., Elm, J., Teiwes, R., Pedersen, H. B., Glasius, M., Ehn, M., and Bilde, M.: The Aarhus Chamber Campaign on Highly Oxygenated Organic Molecules and Aerosols (ACCHA): particle formation, organic acids, and dimer esters from α-pinene ozonolysis at different temperatures, Atmospheric Chemistry and Physics, 20, 12549-12567, 10.5194/acp-20-12549-2020, 2020.

Kürten, A., Williamson, C., Almeida, J., Kirkby, J., and Curtius, J.: On the derivation of particle nucleation rates from experimental formation

595 rates, Atmospheric Chemistry and Physics, 15, 4063-4075, 10.5194/acp-15-4063-2015, 2015.

Lee, A., Goldstein, A. H., Kroll, J. H., Ng, N. L., Varutbangkul, V., Flagan, R. C., and Seinfeld, J. H.: Gas-phase products and secondary aerosol yields from the photooxidation of 16 different terpenes, Journal of Geophysical Research: Atmospheres, 111, 2006.

Li, X., Chee, S., Hao, J., Abbatt, J. P. D., Jiang, J., and Smith, J. N.: Relative humidity effect on the formation of highly oxidized molecules and new particles during monoterpene oxidation, Atmospheric Chemistry and Physics, 19, 1555-1570, 10.5194/acp-19-1555-2019, 2019.

600 Liu, J., D'Ambro, E. L., Lee, B. H., Schobesberger, S., Bell, D. M., Zaveri, R. A., Zelenyuk, A., Thornton, J. A., and Shilling, J. E.: Monoterpene Photooxidation in a Continuous-Flow Chamber: SOA Yields and Impacts of Oxidants, NOx, and VOC Precursors, Environmental Science & Technology, 56, 12066-12076, 10.1021/acs.est.2c02630, 2022.

Ma, Y., Porter, R. A., Chappell, D., Russell, A. T., and Marston, G.: Mechanisms for the formation of organic acids in the gas-phase ozonolysis of 3-carene, Physical Chemistry Chemical Physics, 11, 4184-4197, 10.1039/b818750a, 2009.

605 Mentel, T. F., Springer, M., Ehn, M., Kleist, E., Pullinen, I., Kurtén, T., Rissanen, M., Wahner, A., and Wildt, J.: Formation of highly oxidized multifunctional compounds: autoxidation of peroxy radicals formed in the ozonolysis of alkenes – deduced from structure–product relationships, Atmospheric Chemistry and Phyics, 15, 6745-6765, 10.5194/acp-15-6745-2015, 2015.

Molteni, U., Simon, M., Heinritzi, M., Hoyle, C. R., Bernhammer, A.-K., Bianchi, F., Breitenlechner, M., Brilke, S., Dias, A., Duplissy, J., 610 Frege, C., Gordon, H., Heyn, C., Jokinen, T., Kürten, A., Lehtipalo, K., Makhmutov, V., Petäjä, T., Pieber, S. M., Praplan, A. P., Schobesberger, S., Steiner, G., Stozhkov, Y., Tomé, A., Tröstl, J., Wagner, A. C., Wagner, R., Williamson, C., Yan, C., Baltensperger, U., Curtius, J., Donahue, N. M., Hansel, A., Kirkby, J., Kulmala, M., Worsnop, D. R., and Dommen, J.: Formation of Highly Oxygenated Organic Molecules from α-Pinene Ozonolysis: Chemical Characteristics, Mechanism, and Kinetic Model Development, ACS Earth and Space Chemistry, 3, 873-883, 10.1021/acsearthspacechem.9b00035, 2019.

Nie, W., Yan, C., Yang, L., Roldin, P., Liu, Y., Vogel, A. L., Molteni, U., Stolzenburg, D., Finkenzeller, H., Amorim, A., Bianchi, F., 615 Curtius, J., Dada, L., Draper, D. C., Duplissy, J., Hansel, A., He, X.-C., Hofbauer, V., Jokinen, T., Kim, C., Lehtipalo, K., Nichman, L., Mauldin, R. L., Makhmutov, V., Mentler, B., Mizelli-Ojdanic, A., Petäjä, T., Quéléver, L. L. J., Schallhart, S., Simon, M., Tauber, C., Tomé, A., Volkamer, R., Wagner, A. C., Wagner, R., Wang, M., Ye, P., Li, H., Huang, W., Qi, X., Lou, S., Liu, T., Chi, X., Dommen, J., Baltensperger, U., El Haddad, I., Kirkby, J., Worsnop, D., Kulmala, M., Donahue, N. M., Ehn, M., and Ding, A.: NO at low concentration can enhance the formation of highly oxygenated biogenic molecules in the atmosphere, Nature Communications, 14, 3347, 10.1038/s41467-620 023-39066-4, 2023.

Peräkylä, O., Riva, M., Heikkinen, L., Quéléver, L., Roldin, P., and Ehn, M.: Experimental investigation into the volatilities of highly oxygenated organic molecules (HOMs), Atmospheric Chemistry and Physics, 20, 649-669, 10.5194/acp-20-649-2020, 2020.

Peräkylä, O., Berndt, T., Franzon, L., Hasan, G., Meder, M., Valiev, R. R., Daub, C. D., Varelas, J. G., Geiger, F. M., Thomson, R. J., Rissanen, M., Kurtén, T., and Ehn, M.: Large Gas-Phase Source of Esters and Other Accretion Products in the Atmosphere, Journal of the 625 American Chemical Society, 145, 7780-7790, 10.1021/jacs.2c10398, 2023.

Praske, E., Crounse, J. D., Bates, K. H., Kurtén, T., Kjaergaard, H. G., and Wennberg, P. O.: Atmospheric Fate of Methyl Vinyl Ketone: Peroxy Radical Reactions with NO and HO2, The Journal of Physical Chemistry A, 119, 4562-4572, 10.1021/jp5107058, 2015.

Pye, H. O. T., Chan, A. W. H., Barkley, M. P., and Seinfeld, J. H.: Global modeling of organic aerosol: the importance of reactive nitrogen (NOx and NO3), Atmospheric Chemistry and Physics, 10, 11261-11276, 10.5194/acp-10-11261-2010, 2010.

630 Quéléver, L. L. J., Kristensen, K., Normann Jensen, L., Rosati, B., Teiwes, R., Daellenbach, K. R., Peräkylä, O., Roldin, P., Bossi, R., Pedersen, H. B., Glasius, M., Bilde, M., and Ehn, M.: Effect of temperature on the formation of highly oxygenated organic molecules (HOMs) from alpha-pinene ozonolysis, Atmospheric Chemistry and Physics, 19, 7609-7625, 10.5194/acp-19-7609-2019, 2019.

Rissanen, M. P., Kurten, T., Sipila, M., Thornton, J. A., Kangasluoma, J., Sarnela, N., Junninen, H., Jorgensen, S., Schallhart, S., Kajos, M. K., Taipale, R., Springer, M., Mentel, T. F., Ruuskanen, T., Petaja, T., Worsnop, D. R., Kjaergaard, H. G., and Ehn, M.: The formation of 635 highly oxidized multifunctional products in the ozonolysis of cyclohexene, Journal of the American Chemical Society, 136, 15596-15606, 10.1021/ja507146s, 2014.

Roldin, P., Eriksson, A. C., Nordin, E. Z., Hermansson, E., Mogensen, D., Rusanen, A., Boy, M., Swietlicki, E., Svenningsson, B., Zelenyuk, A., and Pagels, J.: Modelling non-equilibrium secondary organic aerosol formation and evaporation with the aerosol dynamics, gas- and particle-phase chemistry kinetic multilayer model ADCHAM, Atmospheric Chemistry and Phyics, 14, 7953-7993, 10.5194/acp-14-7953-640 2014, 2014.

Roldin, P., Ehn, M., Kurtén, T., Olenius, T., Rissanen, M. P., Sarnela, N., Elm, J., Rantala, P., Hao, L., Hyttinen, N., Heikkinen, L., Worsnop, D. R., Pichelstorfer, L., Xavier, C., Clusius, P., Östrom, E., Petäjä, T., Kulmala, M., Vehkamäki, H., Virtanen, A., Riipinen, I., and Boy, M.: The role of highly oxygenated organic molecules in the Boreal aerosol-cloud-climate system, Nature Communications, 10, 4370, 10.1038/s41467-019-12338-8, 2019.

645 Saathoff, H., Naumann, K. H., Möhler, O., Jonsson, Å. M., Hallquist, M., Kiendler-Scharr, A., Mentel, T. F., Tillmann, R., and Schurath, U.: Temperature dependence of yields of secondary organic aerosols from the ozonolysis of α-pinene and limonene, Atmospheric Chemistry and Physics, 9, 1551-1577, 10.5194/acp-9-1551-2009, 2009.

Schwantes, R. H., Teng, A. P., Nguyen, T. B., Coggon, M. M., Crounse, J. D., St. Clair, J. M., Zhang, X., Schilling, K. A., Seinfeld, J. H., and Wennberg, P. O.: Isoprene NO3 Oxidation Products from the RO2 + HO2 Pathway, The Journal of Physical Chemistry A, 119, 10158-650 10171, 10.1021/acs.jpca.5b06355, 2015.

Shiraiwa, M., Ueda, K., Pozzer, A., Lammel, G., Kampf, C. J., Fushimi, A., Enami, S., Arangio, A. M., Fröhlich-Nowoisky, J., Fujitani, Y., Furuyama, A., Lakey, P. S. J., Lelieveld, J., Lucas, K., Morino, Y., Pöschl, U., Takahama, S., Takami, A., Tong, H., Weber, B., Yoshino, A., and Sato, K.: Aerosol Health Effects from Molecular to Global Scales, Environmental Science & Technology, 51, 13545-13567, 10.1021/acs.est.7b04417, 2017.

655 Shrivastava, M., Cappa, C. D., Fan, J., Goldstein, A. H., Guenther, A. B., Jimenez, J. L., Kuang, C., Laskin, A., Martin, S. T., and Ng, N. L.: Recent advances in understanding secondary organic aerosol: Implications for global climate forcing, Reviews of Geophysics, 55, 509-559, 2017.

Simon, M., Dada, L., Heinritzi, M., Scholz, W., Stolzenburg, D., Fischer, L., Wagner, A. C., Kürten, A., Rörup, B., He, X. C., Almeida, J., Baalbaki, R., Baccarini, A., Bauer, P. S., Beck, L., Bergen, A., Bianchi, F., Bräkling, S., Brilke, S., Caudillo, L., Chen, D., Chu, B., Dias, 660 A., Draper, D. C., Duplissy, J., El-Haddad, I., Finkenzeller, H., Frege, C., Gonzalez-Carracedo, L., Gordon, H., Granzin, M., Hakala, J., Hofbauer, V., Hoyle, C. R., Kim, C., Kong, W., Lamkaddam, H., Lee, C. P., Lehtipalo, K., Leiminger, M., Mai, H., Manninen, H. E., Marie, G., Marten, R., Mentler, B., Molteni, U., Nichman, L., Nie, W., Ojdanic, A., Onnela, A., Partoll, E., Petäjä, T., Pfeifer, J., Philippov, M., Quéléver, L. L. J., Ranjithkumar, A., Rissanen, M. P., Schallhart, S., Schobesberger, S., Schuchmann, S., Shen, J., Sipilä, M., Steiner, G., Stozhkov, Y., Tauber, C., Tham, Y. J., Tomé, A. R., Vazquez-Pufleau, M., Vogel, A. L., Wagner, R., Wang, M., Wang, D. S., Wang, Y., 665 Weber, S. K., Wu, Y., Xiao, M., Yan, C., Ye, P., Ye, Q., Zauner-Wieczorek, M., Zhou, X., Baltensperger, U., Dommen, J., Flagan, R. C., Hansel, A., Kulmala, M., Volkamer, R., Winkler, P. M., Worsnop, D. R., Donahue, N. M., Kirkby, J., and Curtius, J.: Molecular understanding of new-particle formation from α-pinene between −50 and +25 °C, Atmospheric Chemistry and Physics, 20, 9183-9207, 10.5194/acp-20-9183-2020, 2020.

Sindelarova, K., Granier, C., Bouarar, I., Guenther, A., Tilmes, S., Stavrakou, T., Müller, J. F., Kuhn, U., Stefani, P., and Knorr, W.: Global 670 data set of biogenic VOC emissions calculated by the MEGAN model over the last 30 years, Atmospheric Chemistry and Physics, 14, 9317-9341, 10.5194/acp-14-9317-2014, 2014.

Thomsen, D., Elm, J., Rosati, B., Skønager, J. T., Bilde, M., and Glasius, M.: Large Discrepancy in the Formation of Secondary Organic Aerosols from Structurally Similar Monoterpenes, ACS Earth and Space Chemistry, 5, 632-644, 10.1021/acsearthspacechem.0c00332, 2021.

Thomsen, D., Iversen, E. M., Skønager, J. T., Luo, Y., Li, L., Roldin, P., Priestley, M., Pedersen, H. B., Hallquist, M., and Ehn, M.: The 675 effect of temperature and relative humidity on secondary organic aerosol formation from ozonolysis of Δ3-carene, Environmental Science: Atmospheres, 4, 88-103, 2024.

Thomsen, D., Thomsen, L. D., Iversen, E. M., Björgvinsdóttir, T. N., Vinther, S. F., Skønager, J. T., Hoffmann, T., Elm, J., Bilde, M., and Glasius, M.: Ozonolysis of α-Pinene and Δ3-Carene Mixtures: Formation of Dimers with Two Precursors, Environmental Science & Technology, 10.1021/acs.est.2c04786, 2022.

680 Tillmann, R., Hallquist, M., Jonsson, Å., Kiendler-Scharr, A., Saathoff, H., Iinuma, Y., and Mentel, T. F.: Influence of relative humidity and temperature on the production of pinonaldehyde and OH radicals from the ozonolysis of α-pinene, Atmospheric Chemistry and Physics, 10, 7057-7072, 2010.

Valiev, R. R., Hasan, G., Salo, V.-T., Kubečka, J., and Kurten, T.: Intersystem Crossings Drive Atmospheric Gas-Phase Dimer Formation, The Journal of Physical Chemistry A, 123, 6596-6604, 10.1021/acs.jpca.9b02559, 2019.

685 Vereecken, L. and Peeters, J.: Decomposition of substituted alkoxy radicals—part I: a generalized structure–activity relationship for reaction barrier heights, Physical Chemistry Chemical Physics, 11, 9062-9074, 2009.

Wang, L., Liu, Y., and Wang, L.: Ozonolysis of 3-carene in the atmosphere. Formation mechanism of hydroxyl radical and secondary ozonides, Physical Chemistry Chemical Physics, 21, 8081-8091, 10.1039/c8cp07195k, 2019.

Warren, B., Austin, R. L., and Cocker, D. R.: Temperature dependence of secondary organic aerosol, Atmospheric Environment, 43, 3548-690 3555, https://doi.org/10.1016/j.atmosenv.2009.04.011, 2009.

Zhao, J., Häkkinen, E., Graeffe, F., Krechmer, J. E., Canagaratna, M. R., Worsnop, D. R., Kangasluoma, J., and Ehn, M.: A combined gas- and particle-phase analysis of highly oxygenated organic molecules (HOMs) from α-pinene ozonolysis, Atmospheric Chemistry and Physics, 23, 3707-3730, 10.5194/acp-23-3707-2023, 2023.